Article

A brain reward circuit inhibited by next-generation weight-loss drugs in mice

https://doi.org/10.1038/s41586-026-10444-4

Received: 12 December 2024

Accepted: 24 March 2026

Published online: 06 May 2026

Open access

Check for updates

Elizabeth N. Godschall[1,12], Taha Bugra Gungul[1,12], Isabelle R. Sajonia[1,12], Aleyna K. Buyukaksakal[1], Orien Li[1], Sophia Ogilvie[1], Austin B. Keeler[1], Guilian Tian[2], Yu Shi[1], Omar Koita[3,4], Chloe Xinzhu Guo[1], Tyler C. J. Deutsch[5,6], Eric J. Steacy[5,7], Maisie Crook[1], YuChen Zhang[7], Nicholas J. Conley[1,7], Gulsun Memi[1,8], Addison N. Webster[1,7], O. Yipkin Calhan[1], Weile Liu[1], Amani Akkoub[1], Karan Malik[1], Kaleigh I. West[1], Sara Michel-Le[1], Arun Karthikeyan[1], Grace van Gerven[1], Olivia A. Dell'Aglio[1], Kevin T. Beier[2], Larry S. Zweifel[3,4], Manoj K. Patel[5,7], John N. Campbell[1,7,9], Christopher D. Deppmann[1,7,9,10,11] ✉ & Ali D. Güler[1,7,9] ✉

Glucagon-like peptide 1 receptor agonists (GLP1RAs) effectively reduce body weight and improve metabolic outcomes; however, established peptide-based therapies require injections and are complex to manufacture[1–3]. Small-molecule GLP1RAs promise oral bioavailability and scalable manufacturing, but their selective binding to human versus rodent receptors has limited mechanistic studies[4–9]. Here we developed humanized GLP1R mouse models to investigate how small-molecule GLP1RAs influence feeding behaviour. We found that these compounds regulate both homeostatic and hedonic feeding through parallel neural circuits. Beyond engaging canonical hypothalamic and hindbrain networks that control metabolic homeostasis, GLP1RAs recruit a discrete population of *Glp1r*-expressing neurons in the central amygdala, which selectively suppress the consumption of palatable foods by reducing dopamine release in the nucleus accumbens. Stimulating these central amygdalar neurons curtails hedonic feeding, whereas targeted deletion of the receptor in this cell population specifically diminishes the anorectic efficacy of GLP1RAs for reward-driven intake. These findings identify a neural circuit through which small-molecule GLP1RAs modulate reward processing, with implications for the treatment of substance-use disorder and binge eating.

Glucagon-like peptide 1 receptor agonists (GLP1RAs) have emerged as highly effective treatments for obesity and diabetes. Beyond their metabolic benefits, these drugs show promise for treating conditions such as substance-use disorders, indicating central reward circuit engagement[1–3,10,11]. Although GLP1RAs are known to engage hypothalamic and hindbrain regions to suppress homeostatic feeding[12–18], their effect on the neural circuits that drive hedonic food consumption remains mostly unknown. Gaining an understanding of these mechanisms is especially relevant today, because small-molecule GLP1RAs are poised to expand access to this transformative class of medications[4].

Next-generation GLP1RAs such as danuglipron (PF-06882961) and orforglipron (LY3502970) offer oral bioavailability and scalable manufacturing[4–7] (Fig. 1a). But these compounds show species-specific binding: many small-molecule GLP1RAs activate human but not rodent GLP1R, precluding preclinical investigation of their mechanisms of action[4,7–9,19]. Notably, orforglipron was recently approved by the FDA for weight management; however, the development of danuglipron was discontinued owing to side effects that preclinical profiling might have identified[4–6].

To overcome the species specificity of small-molecule GLP1RAs, here we engineered humanized GLP1R mouse models. Through integrated behavioural, neuroanatomical and functional analyses, we uncover a multi-synaptic hindbrain–amygdala–midbrain circuit that modulates reward-driven feeding through striatal dopaminergic signalling. This discovery reveals how GLP1R signalling influences both feeding behaviour and reward processes, highlighting both the therapeutic potential of these treatments and the need for caution as they see broader use[3,10,11].

Humanized *Glp1r*^{S33W} mice

Although peptide GLP1RAs, like liraglutide, reduce food consumption in C57BL/6J mice, many small-molecule GLP1RAs do not effectively activate rodent GLP1R (Fig. 1b), owing to a single amino acid difference[8,9,19] (tryptophan in humans and serine in rodents at position 33; Fig. 1c).

[1]Department of Biology, University of Virginia, Charlottesville, VA, USA. [2]Department of Physiology and Biophysics, University of California, Irvine, Irvine, CA, USA. [3]Department of Pharmacology, University of Washington, Seattle, WA, USA. [4]Department of Psychiatry, University of Washington, Seattle, WA, USA. [5]Department of Anesthesiology, University of Virginia, Charlottesville, VA, USA. [6]Edward Via College of Osteopathic Medicine, Blacksburg, VA, USA. [7]Neuroscience Graduate Program, University of Virginia, Charlottesville, VA, USA. [8]Department of Physiology, School of Medicine, Adiyaman University, Adiyaman, Turkey. [9]Program in Fundamental Neuroscience, University of Virginia, Charlottesville, VA, USA. [10]Department of Cell Biology, University of Virginia, Charlottesville, VA, USA. [11]Department of Biomedical Engineering, University of Virginia, Charlottesville, VA, USA. [12]These authors contributed equally: Elizabeth N. Godschall, Taha Bugra Gungul, Isabelle R. Sajonia. ✉e-mail: deppmann@virginia.edu; aguler@virginia.edu

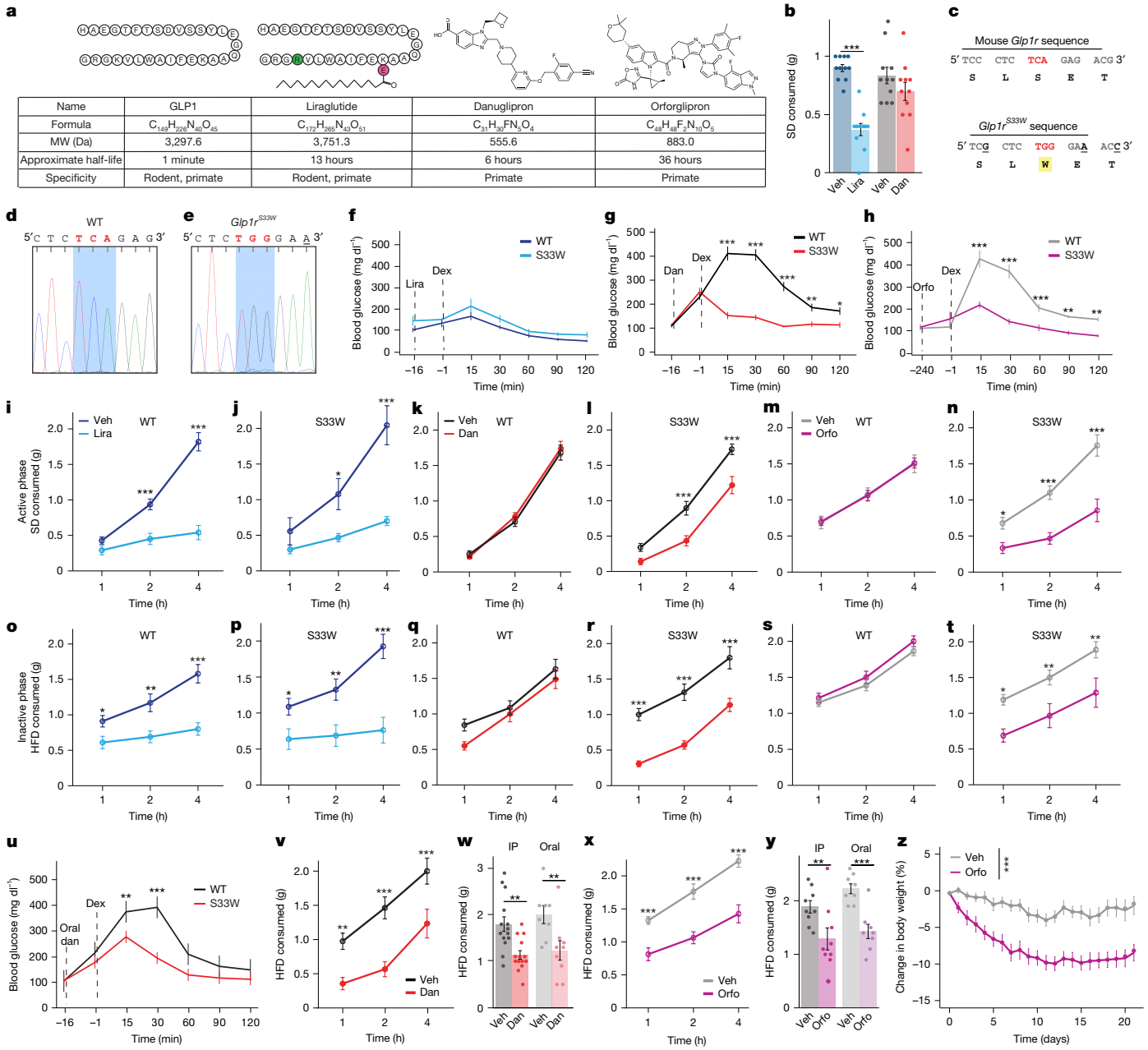

Name	GLP1	Liraglutide	Danuglipron	Orforglipron
Formula	$C_{149}H_{226}N_{40}O_{45}$	$C_{172}H_{265}N_{43}O_{51}$	$C_{31}H_{30}FN_5O_4$	$C_{48}H_{48}F_2N_{10}O_5$
MW (Da)	3,297.6	3,751.3	555.6	883.0
Approximate half-life	1 minute	13 hours	6 hours	36 hours
Specificity	Rodent, primate	Rodent, primate	Primate	Primate

Fig. 1 | Validation of small-molecule GLP1R agonist-responsive mouse model. a, Characteristics of GLP1, liraglutide, danuglipron and orforglipron. MW, molecular weight. **b**, Two-hour SD intake after treatment with liraglutide (Lira), vehicle (Veh) or danuglipron (Dan) ($n = 11$ per group). **c**, Serine (TCA or S) to tryptophan (TGG or W) CRISPR-mediated substitution in *Glp1r*^{S33W} mice. **d**,**e**, Sequencing chromatograms of WT mouse *Glp1r* (**d**) and *Glp1r*^{S33W} (**e**). **f**–**h**, Glucose (dextrose; Dex) tolerance test. Blood glucose levels on liraglutide (**f**; WT $n = 8$, *Glp1r*^{S33W} $n = 6$), danuglipron (**g**; WT $n = 9$, *Glp1r*^{S33W} $n = 6$) or orforglipron (Orfo) (**h**; WT $n = 5$, *Glp1r*^{S33W} $n = 5$) in WT and *Glp1r*^{S33W} mice. **i**–**n**, SD intake after treatment with liraglutide (**i**,**j**; WT $n = 10$, *Glp1r*^{S33W} $n = 9$), danuglipron (**k**,**l**; WT $n = 16$, *Glp1r*^{S33W} $n = 15$), orforglipron (**m**,**n**; WT $n = 8$, *Glp1r*^{S33W} $n = 9$) or their vehicle controls in WT and *Glp1r*^{S33W} mice. **o**–**t**, HFD intake after treatment with liraglutide (**o**,**p**; WT $n = 10$, *Glp1r*^{S33W} $n = 8$), danuglipron (**q**,**r**; WT $n = 16$, *Glp1r*^{S33W} $n = 14$), orforglipron (**s**,**t**; WT $n = 8$, *Glp1r*^{S33W} $n = 9$) or their vehicle controls in WT and *Glp1r*^{S33W} mice. **u**, GTT after oral administration of danuglipron (Oral dan) in *Glp1r*^{S33W} and WT mice ($n = 6$ per group). **v**,**x**, HFD intake after oral administration of danuglipron ($n = 9$) or vehicle ($n = 8$) (**v**) or oral administration of orforglipron ($n = 8$) or vehicle ($n = 8$) (**x**) in *Glp1r*^{S33W} mice. **w**,**y**, Four-hour food intake (HFD) after intraperitoneal (IP) or oral administration of danuglipron (**w**; IP $n = 14$ per injection, oral vehicle $n = 8$, oral dan $n = 9$) or orforglipron (**y**; IP $n = 9$ per injection, oral $n = 8$ per injection). **z**, Change in body weight in male mice on HFD (at least 8 weeks) treated with daily (ZT6) orforglipron or vehicle ($n = 10$ per group). All data are mean ± s.e.m. Statistical tests: one-way ANOVA (**b**; two-way ANOVA) with Bonferroni correction (**f**–**z**). $^*P < 0.05$; $^{**}P < 0.01$; $^{***}P < 0.001$. See Supplementary Table 1 for statistical details.

Using CRISPR–Cas9-mediated genome editing, we inserted the S33W mutation into the mouse *Glp1r* locus, effectively humanizing it (Fig. 1d,e). Homozygous humanized *Glp1r* mice (*Glp1r*^{S33W}) and wild-type (WT) littermates showed no differences in respiratory exchange ratio (Extended Data Fig. 1a–d), energy expenditure (Extended Data Fig. 1e–h) or body weight (Extended Data Fig. 1i,j), showing normal metabolic function. To evaluate the functionality of the S33W mutation in vivo, we performed glucose tolerance tests (GTTs) and found that liraglutide improved glucose tolerance in both *Glp1r*^{S33W} mice and WT mice (Fig. 1f), whereas danuglipron and orforglipron were effective only in *Glp1r*^{S33W} mice (Fig. 1g,h). Similar to previously developed rodent models[20,21], these results show that *Glp1r*^{S33W} mice retain responsiveness

to peptide-based GLP1RAs while gaining sensitivity to human-specific small-molecule GLP1RAs, establishing a valuable model system for investigating this next-generation class of drugs.

Beyond their effects on treating type II diabetes, GLP1RAs induce significant weight loss[1,5]. To systematically characterize their effects on distinct feeding modalities, we used parallel behavioural paradigms examining both homeostatic and hedonic feeding patterns. Homeostatic feeding was quantified through consumption of a standard diet (SD) during the active phase (zeitgeber time (ZT) 12–16), and hedonic feeding was assessed through intake of a high-fat diet (HFD) during the rest phase (ZT2–ZT6), when baseline SD consumption is negligible[22,23]. After determining the minimal dose of danuglipron that robustly suppressed intake (Extended Data Fig. 1k), we selected orforglipron and liraglutide doses to match its anorectic effect. At these doses, all three agonists markedly reduced active-phase SD consumption (Fig. 1j,l,n) and rest-phase HFD feeding (Fig. 1p,r,t) in *Glp1r*^{S33W} mice. SD consumption after an overnight fast was likewise suppressed by each treatment (Extended Data Fig. 1l–n). As predicted by species-specific receptor activation, WT mice exhibited reduced SD (Fig. 1i,k,m) and HFD (Fig. 1o,q,s) intake only with liraglutide. Notably, both liraglutide and orforglipron yielded a sustained 24-h inhibition of food intake (Extended Data Fig. 1o-q), consistent with their extended pharmacokinetic profiles relative to danuglipron (Fig. 1a). To validate the clinical relevance of these orally bioavailable small-molecule GLP1RAs, we confirmed that oral danuglipron significantly reduced blood glucose levels (Fig. 1u) and acute HFD intake, to comparable extents to that produced by intraperitoneal injection (Fig. 1v,w). Similarly, oral orforglipron inhibited acute HFD intake (Fig. 1x,y), and its chronic daily administration in overweight *Glp1r*^{S33W} mice significantly reduced body weight, compared with vehicle controls (Fig. 1z).

Behavioural profiling in *Glp1r*^{S33W} mice

Because nausea often limits the clinical tolerance of GLP1RAs, we sought to distinguish nausea-like from satiety behaviours induced by peptide and small-molecule drugs. Although conditioned taste avoidance was evident after treatment with lithium chloride (LiCl; a nausea-inducing drug) and liraglutide, as previously reported[18], this assay did not detect malaise in danuglipron- or orforglipron-treated mice (Extended Data Fig. 2a–c). Because danuglipron and orforglipron also did not alter anxiety-like behaviour in the open field test or elevated plus maze (Extended Data Fig. 2d–m), we were able to use high-resolution home-cage tracking to capture nuanced behavioural differences (Fig. 2a,b and Supplementary Fig. 1). We first generated a 'nausea' reference, by treating mice with LiCl, and a 'satiety' reference, by pre-feeding mice a HFD for one hour before recording. Using these benchmarks, we compared home-cage behaviour after each GLP1RA to determine which profile it most closely mimicked. Mice were video-recorded for two hours (ZT12–ZT14) in their home cages after each treatment (Supplementary Fig. 1). Behavioural states were quantified using pose estimation (SLEAP)[24] of nine keypoints and a probabilistic classification model (Keypoint-MoSeq)[25], which identified 91 behavioural syllables (Fig. 2c and Supplementary Figs. 2 and 3).

Syllable-level analysis revealed distinct behavioural alterations: the use of 28 syllables was significantly modulated by LiCl, 25 by liraglutide, 22 by danuglipron and 13 by orforglipron. LiCl, liraglutide and danuglipron generally reduced locomotor syllables (for example, running) but increased non-locomotor behaviours such as grooming, turning and sniffing, relative to vehicle controls (Fig. 2d–f, Supplementary Fig. 4 and Extended Data Fig. 3). Most syllables that were downregulated by orforglipron relative to vehicle corresponded to non-locomotor behaviours (for example, sniffing, grooming and head probing). Among the four treatment groups, 20 syllables exhibited significant drug-induced changes in use that were common to at least two groups. Orforglipron shared only 5 syllables with other treatments, compared with 11 for LiCl, 13 for danuglipron and 17 for liraglutide (Fig. 2e,f and Extended Data Fig. 3).

Transition analysis supported this divergence, with LiCl, liraglutide and danuglipron showing reduced locomotor-to-locomotor transitions and increased transitions to non-locomotor states, suggesting behavioural blunting (Extended Data Fig. 4). To capture higher-order patterns and spatial context, we grouped syllables into five categories—food-motivated, drinking, grooming, movement/exploration and resting/grooming in shelter—on the basis of human annotation, transition-network analysis and location data (Fig. 2g–m). Consistent with reduced intake, all GLP1RAs and LiCl suppressed food-hopper head entries, compared with their respective vehicle controls. However, only LiCl, liraglutide and danuglipron reduced time in food-motivated behaviours, whereas liraglutide and danuglipron also decreased drinking (Fig. 2n–p). LiCl and liraglutide reduced distance travelled and increased grooming, whereas LiCl and danuglipron increased rest in shelter (Fig. 2q,r and Extended Data Fig. 5). By contrast, orforglipron-treated mice maintained a more active, exploratory profile despite reduced food-hopper head entries. Their transition dynamics also differed: fed mice made significantly more rest-to-exploration transitions than did other cohorts (Fig. 2s–x and Extended Data Fig. 6a–x). These grouped-syllable analyses recapitulated the trends observed in the ungrouped syllable frequency and transition data.

To examine behavioural variance independent of feeding, we performed principal component analysis (PCA) on time spent, transition probabilities and bout characteristics for non-food-motivated behaviours. (Fig. 2y and Extended Data Fig. 6y,z). Visually, orforglipron and the fed group occupied distinct regions of PCA space, separate from LiCl, liraglutide and danuglipron, which clustered more closely together. Principal component 1 (PC1) captured the axis separating active and sheltered behaviours: fed and orforglipron grouped towards higher locomotion and exploration, whereas LiCl, danuglipron and liraglutide aligned with increased sheltering and rest. PC2 represented a contrast between drinking behaviour (orforglipron) and grooming behaviour (fed, liraglutide, danuglipron and, partially, LiCl). These patterns align with our syllable- and transition-level analyses. Together, these results show that orforglipron produces a behavioural profile distinct from both nausea-like and satiety states, suggesting that its anorectic effects are separable from aversion.

GLP1RAs induce distinct brain activation

Given the distinct behavioural signatures of peptide and small-molecule GLP1RAs and their differing pharmacokinetic profiles, we investigated the neural substrates mediating their anorectic effects. We examined nuclei that express *Glp1r* and are activated by peptide GLP1RAs: the dorsomedial hypothalamus (DMH), nucleus tractus solitarius (NTS), area postrema (AP) and central amygdala (CeA)[13,15–17,26–28]. We quantified FOS expression as a proxy for GLP1RA-induced neuronal activation in WT and *Glp1r*^{S33W} mice after treatment with vehicle, danuglipron, orforglipron or liraglutide (Fig. 3a–h). In *Glp1r*^{S33W} mice, danuglipron and orforglipron significantly increased FOS in the NTS (Fig. 3f), AP (Fig. 3g) and CeA (Fig. 3h), but not in the DMH (Fig. 3e), compared with WT controls, consistent with previous studies using peptide-based GLP1RAs[13,26,29,30]. As expected, liraglutide induced comparable expression of FOS in both genotypes, and in *Glp1r*^{S33W} mice its pattern closely matched the responses to small-molecule agonists across all regions (Fig. 3e–i), confirming effective binding and activation of the GLP1R^{S33W} variant.

Although AP activation is often associated with nausea and malaise, and NTS activation with satiety-related signalling, these functions are not mutually exclusive, and both nuclei are likely to contribute to multiple aspects of ingestive behaviour[15,31]. Within this framework, we reasoned that differences in the relative recruitment of AP and

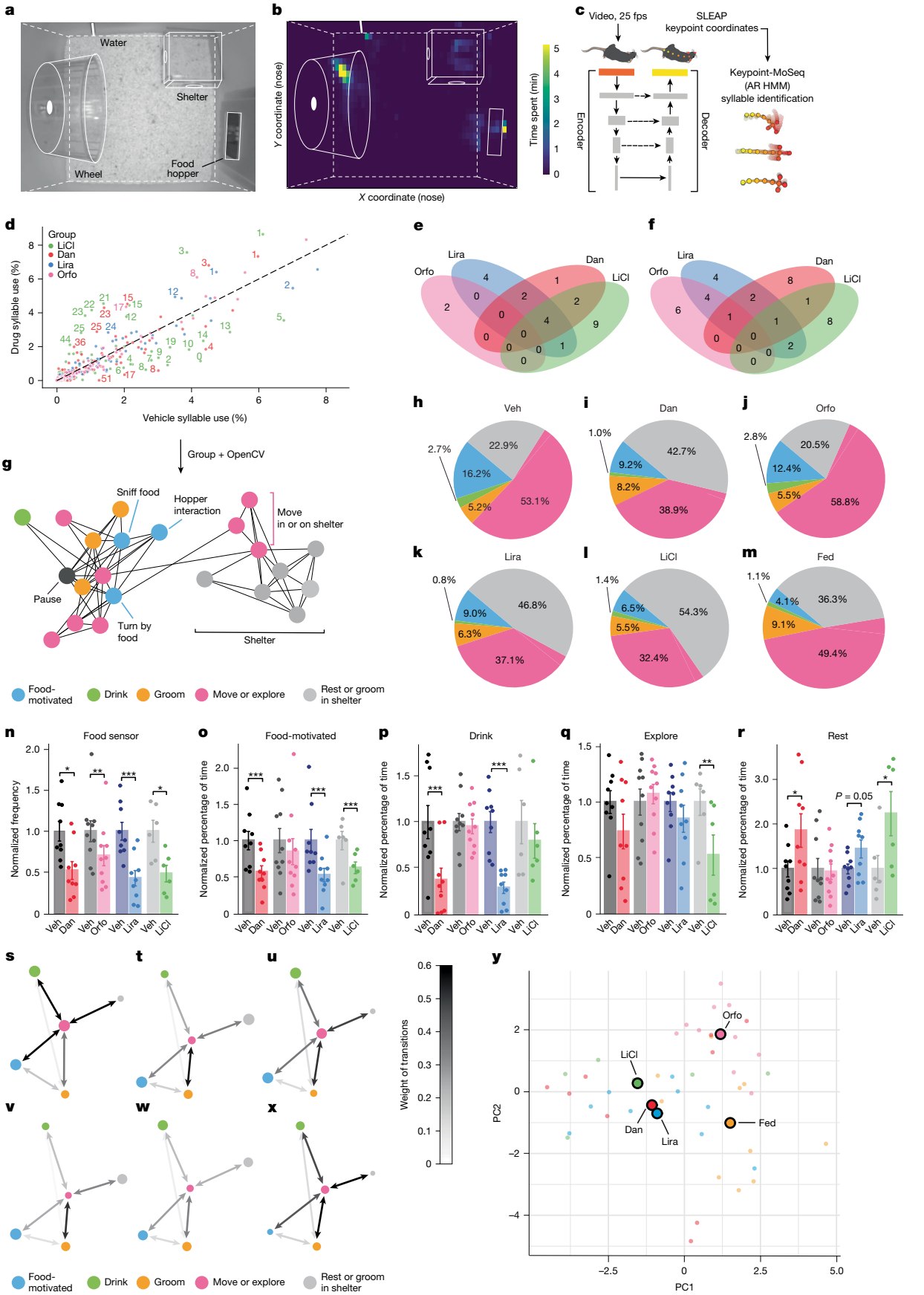

Fig. 2 | See next page for caption.

Fig. 2 | Machine learning-assisted behaviour profiling reveals distinct phenotypes associated with GLP1RAs. a, Home-cage video recording set-up. **b**, Representative heat map of mouse nose location. **c**, Behaviour machine learning analysis pipeline using SLEAP and Keypoint-MoSeq (an autoregressive hidden Markov model (AR HMM))[24,25]. fps, frames per second. **d**, Drug-induced changes in behavioural syllable use (percentage); top 10% of baseline changes labelled by syllable number. **e**,**f**, Venn diagrams of syllables with significant ($P < 0.05$) changes in syllable use (upregulated syllables (**e**) and downregulated syllables (**f**)) versus paired vehicle controls; overlaps indicate shared significant syllable identities across drug groups. **g**, Twenty-two manually annotated behaviours grouped into five state- and location-based categories, and constructed as a transition network. **h**–**m**, Percentage of time spent in each of the five behavioural categories, averaged across mice per condition (vehicle (**h**), danuglipron (**i**), orforglipron (**j**), liraglutide (**k**), LiCl (**l**) and Fed (**m**)). **n**, Food-hopper head entries normalized to vehicle controls. **o**–**r**, Percentage of time spent food seeking (**o**), drinking (**p**), moving or exploring (**q**) and resting or grooming in the shelter (**r**). **s**–**x**, Network analysis of behavioural category transitions (vehicle (**s**), danuglipron (**t**), orforglipron (**u**), liraglutide (**v**), LiCl (**w**) and Fed (**x**)). Transition probabilities were normalized by outgoing transitions per individual, combined across directions (A↔B) and averaged within condition. Node colours indicate behaviours; node size reflects scaled average bout length. Arrow colour reflects transition probability. **y**, PCA of behavioural features excluding food-motivated behaviours. Each dot represents an individual mouse, colour-coded by experimental group. Filled circles indicate group means. PCA was performed on behavioural metrics (duration, transitions and bouts). PCs 1–3 explain 64.6% of the total variance. All data are mean ± s.e.m. Paired *t*-tests were used for **e**–**f**,**n**. For **o**–**r**, a generalized linear mixed-effects model with a beta distribution was fitted to raw proportion data, including a random intercept for mouse ID to account for the paired design. For all panels: Veh, Dan, $n = 9$; Veh, Orfo, $n = 10$; Veh, Lira, $n = 9$; Veh, LiCl, $n = 6$; and Fed, $n = 10$. All statistical tests were two-tailed. $^{*}P < 0.05$, $^{**}P < 0.01$, $^{***}P < 0.001$. The mouse schematic in **c** was sourced from https://scidraw.io/ and reproduced from ref. 51 under a Creative Commons licence CC BY 4.0.

NTS might help to explain the distinct behavioural profiles elicited by different GLP1RAs[5,32]. To test this, we calculated the NTS-to-AP FOS ratio for each treatment. Orforglipron produced a significantly higher NTS-to-AP ratio, reflecting a bias towards NTS-dominant engagement, whereas danuglipron and liraglutide yielded lower ratios that aligned with a more AP-skewed, nausea-like activation profile, in keeping with their distinct pharmacokinetic and signalling properties[7–9] (Fig. 3j). Because these compounds are intended for oral use, we compared intraperitoneal versus oral delivery of danuglipron and orforglipron in *Glp1r*^{S33W} and WT mice to assess how administration route influences the pattern of FOS activation in the hindbrain (Fig. 3k,l). NTS FOS activation in *Glp1r*^{S33W} mice was comparable across routes and drugs (Fig. 3m), but oral danuglipron significantly reduced AP FOS activation, compared with intraperitoneal delivery (Fig. 3n). This is likely to reflect the fact that oral dosing produces slower absorption and lower peak exposure, which might reduce recruitment of AP neurons that are sensitive to circulating factors. Preferential recruitment of NTS over AP might therefore help to limit nausea and malaise—side effects that are often linked to AP engagement—while preserving NTS-linked therapeutic benefits[15].

Small molecules activate GLP1R circuits

To distinguish direct effects of small-molecule GLP1RAs from indirect ones, we used *Glp1r-Cre* mice and a Cre-dependent adeno-associated virus (AAV) expressing full-length human GLP1R (AAV-hSyn-DIO-hGLP1R) (Fig. 4a). In this configuration, expression of human GLP1R is restricted to Cre-positive, endogenously *Glp1r*-expressing neurons in each targeted region (Supplementary Fig. 5a,b), allowing direct assessment of region-specific GLP1R activation. We used danuglipron for these experiments because its fast-onset kinetics facilitated temporal alignment between drug administration, feeding assays and fibre photometry recordings, enabling more precise interpretation of region-specific GLP1R activation[7–9]. In mice with expression of human GLP1R in the basomedial hypothalamus (BMH) (BMH-hGLP1R) (Supplementary Fig. 5c,d), danuglipron significantly decreased active-phase SD intake without affecting rest-phase HFD consumption (Fig. 4c,h), whereas control mice expressing mCherry in the same region showed no changes (Fig. 4b,g). When targeting the DMH, a BMH subnucleus implicated in satiation[16], we observed a similar selective reduction in SD intake (Fig. 4d,i and Supplementary Fig. 5e,f). These results show that DMH GLP1R signalling regulates homeostatic feeding despite the absence of bulk FOS induction (Fig. 3e), possibly owing to microcircuit interactions that mask population-level signals. Targeting the hindbrain NTS–AP complex decreased the consumption of both SD and HFD (Fig. 4e,j and Supplementary Fig. 5g,h), consistent with previous findings on hindbrain GLP1R circuits[15].

Regulation of hedonic feeding by small molecules

Although the CeA has been implicated in feeding behaviour[28,33–37], its role in mediating responses to GLP1RAs remains poorly defined[38]. Our finding that small-molecule GLP1RAs induce FOS expression in the CeA (Fig. 3h) raised several fundamental questions about (1) the functional relevance of CeA^{Glp1r} neurons in feeding behaviour; (2) whether danuglipron can directly activate these deep-brain neurons, despite doubts about its penetration of the blood–brain barrier; and (3) the neurochemical identity of these cells.

To address the functional point, we expressed human GLP1R selectively in the CeA neurons of *Glp1r-Cre* mice (CeA-hGLP1R mice). Notably, danuglipron selectively suppressed HFD intake without altering SD consumption in these mice (Fig. 4f,k and Supplementary Fig. 5i,j). We confirmed this effect using an orthogonal viral strategy: Cre-dependent expression of the danuglipron-sensitive mouse *Glp1r*^{S33W} variant in CeA neurons reproduced HFD suppression, whereas expression of the WT mouse *Glp1r* served as an unresponsive control (Extended Data Fig. 7a–d). These data identify CeA^{Glp1r} neurons as a previously unrecognized yet crucial substrate for GLP1RA-mediated suppression of hedonic feeding.

To characterize the neurochemical properties of these cells, we combined bioinformatic and electrophysiological approaches. An analysis of published CeA single-nucleus RNA sequencing data revealed that *Glp1r*-expressing neurons co-express GABAergic markers, lack glutamatergic markers and cluster with CeA neurons that express the vitamin D receptor, *Vdr*[39] (Supplementary Fig. 6). Spatial transcriptomic analysis (Allen Brain Atlas MERFISH) suggests that *Glp1r* expression in the CeA is not restricted to a single neuronal subtype[40] (Supplementary Fig. 7). Consistent with this, RNAscope showed that CeA^{Glp1r} neurons partially overlap (around 30% co-expression) with *Pnoc*-expressing neurons (Supplementary Fig. 7g–n), which have been implicated in promoting hedonic feeding[37,38]. These findings highlight the cellular heterogeneity of CeA^{Glp1r} neurons and their potential importance in regulating hedonic feeding. To assess the neurophysiological effect of danuglipron on human-GLP1R-expressing neurons, we performed whole-cell patch-clamp recordings after co-injection of AAV-DIO-hGLP1R and AAV-DIO-eYFP into the amygdala of *Glp1r-Cre* mice (Extended Data Fig. 7e–j). In acute slices, we measured the resting membrane potential before and during bath application of danuglipron (30 μM; Extended Data Fig. 7h,i). As expected from G_s–cAMP-coupled activation, danuglipron induced significant depolarization in human GLP1R neurons, compared with mouse GLP1R controls (Extended Data Fig. 7j). Within-cell analyses in human-GLP1R-expressing neurons confirmed depolarization from baseline and a reduced time to spike threshold during current injection, indicating increased excitability following danuglipron application (Extended Data Fig. 7k–m).

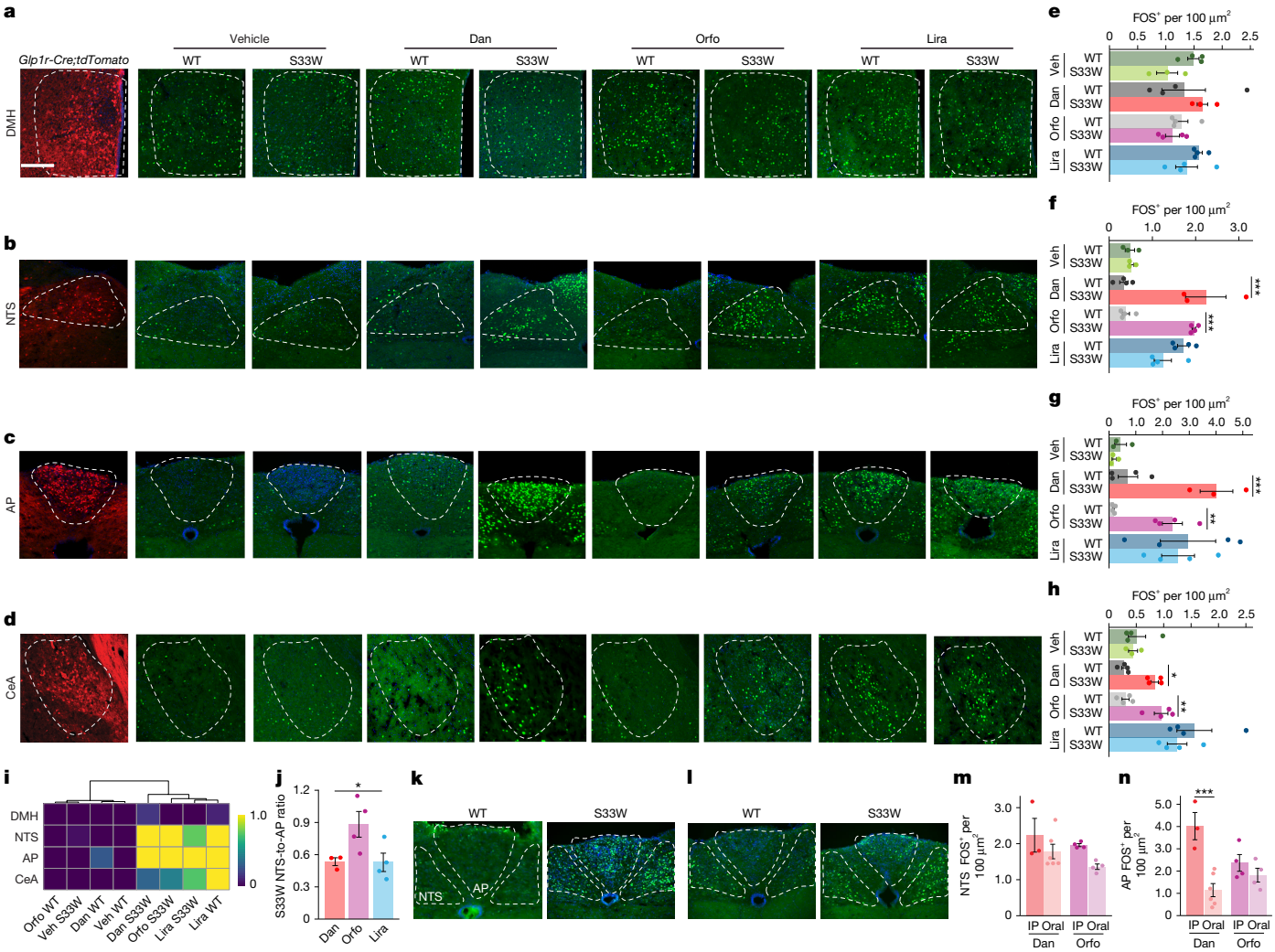

Fig. 3 | GLP1RA activation across targeted GLP1R-expressing brain regions. **a**–**d**, *Glp1r-Cre;tdTomato* mice mark GLP1R-positive neurons; FOS activation after treatment with vehicle, danuglipron, orforglipron or liraglutide in WT and *Glp1r*^{S33W} mice in the DMH (**a**), NTS (**b**), AP (**c**) or CeA (**d**). Scale bar, 200 µm. **e**–**h**, Quantification of FOS in the DMH (**e**), NTS (**f**), AP (**g**) and CeA (**h**). Vehicle: DMH and CeA, $n = 4$ (WT), $n = 3$ (S33W); NTS and AP, $n = 3$ per genotype. Orforglipron and liraglutide: $n = 4$ per genotype in all regions. Danuglipron: NTS and AP, $n = 4$ (WT), $n = 3$ (S33W); DMH and CeA, $n = 4$ per genotype. **i**, Heat map of FOS activity in brain regions of interest across drug and vehicle conditions, normalized to WT vehicle. **j**, Ratio of NTS to AP FOS activation in *Glp1r*^{S33W} mice after treatment with danuglipron ($n = 3$), orforglipron ($n = 4$) or liraglutide ($n = 4$). **k**,**l**, Neuronal FOS activation in the NTS and AP after administration of danuglipron (**k**) or orforglipron (**l**) to WT and *Glp1r*^{S33W} mice by oral gavage. **m**,**n**, Quantification of FOS expression in the NTS (**m**) or AP (**n**) after IP or oral delivery of danuglipron or orforglipron in *Glp1r*^{S33W} mice. Sample sizes: danuglipron oral, $n = 6$ (NTS and AP); danuglipron IP, $n = 3$ (NTS and AP); all other groups, $n = 4$. Data are mean ± s.e.m. Statistical tests: two-way ANOVA with Bonferroni correction (**e**–**h**,**m**,**n**); Kruskal–Wallis test (**j**). $^{*}P < 0.05$; $^{**}P < 0.01$; $^{***}P < 0.001$.

Danuglipron's low molecular weight (555.6 Da) compared with peptide-based GLP1RAs, and its ability to suppress hedonic feeding in mice expressing human GLP1R only in CeA^{Glp1r} neurons (Fig. 4k), suggest that it crosses the blood–brain barrier to act on deep targets beyond the circumventricular organs (brain regions that lack a tight blood–brain barrier). Although the level of central nervous system penetration by different GLP1RAs remains debated[13,26,38,41,42], defining their direct engagement of deep nuclei is essential. To demonstrate danuglipron's direct activation of central GLP1R neurons in freely moving mice, we used two complementary approaches. First, we injected AAV-DIO-hGLP1R (where the h prefix indicates human) into one CeA and AAV-DIO-mGLP1R (where the m prefix indicates mouse) into the contralateral CeA of the same *Glp1r-Cre* mice (Fig. 4l). After treatment with danuglipron, FOS colocalization was significantly greater in human-GLP1R-expressing neurons versus the mouse GLP1R side (Fig. 4m–o), confirming receptor-specific activation in deep-brain tissue. Second, we co-expressed GCaMP7s with either human GLP1R or mouse GLP1R in the CeA of *Glp1r-Cre* mice and recorded calcium transients through fibre photometry (Fig. 4p and Extended Data Fig. 8a–g). Building on previous work and our own finding that peptide GLP1RAs induce CeA FOS expression in WT mice[13,26,29,30] (Fig. 3d,h), liraglutide evoked robust calcium responses in CeA-hGLP1R mice, as expected (Extended Data Fig. 8h–j). Of note, danuglipron similarly evoked significant calcium transients only in human-GLP1R-expressing mice, with no evoked responses in mouse-GLP1R-expressing negative controls (Fig. 4q–t and Extended Data Fig. 8e–g). Because fibre photometry measures population-level activity, we cannot rule out that different subsets of CeA^{Glp1r} neurons are differentially recruited by individual GLP1RAs, with similar bulk responses arising from overlapping but non-identical populations. Nonetheless, these findings show that danuglipron crosses the blood–brain barrier to directly activate deep-brain CeA neurons through the human GLP1R.

To define the physiological role of CeA^{Glp1r} neurons in hedonic feeding, we expressed ChR2 in the CeA of *Glp1r-Cre* mice (Supplementary

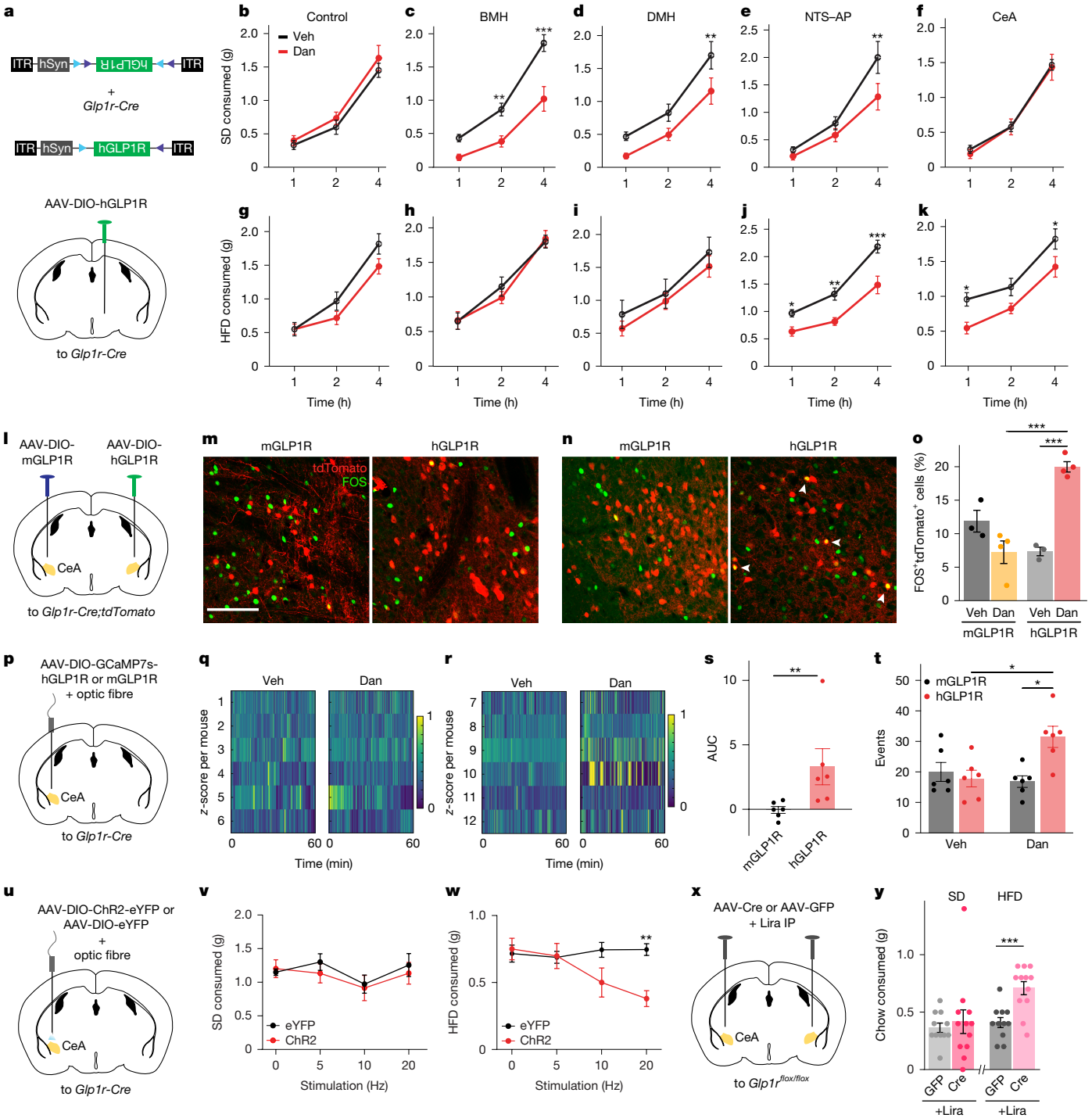

Fig. 4 | GLP1R activation in the CeA inhibits hedonic food intake. a, Schematic of AAV-DIO-hGLP1R delivery to the BMH. **b**–**k**, Homeostatic SD (**b**–**f**) or hedonic HFD (**g**–**k**) intake after treatment with vehicle or danuglipron in *Glp1r-Cre* mice expressing AAV-DIO-mCherry in the BMH (BMH-mCherry, $n = 6$) (**b**,**g**) or expressing AAV-DIO-hGLP1R (BMH-hGLP1R, $n = 10$) in the BMH (**c**,**h**), DMH ($n = 7$) (**d**,**i**), NTS–AP ($n = 6$) (**e**,**j**) or CeA ($n = 9$) (**f**,**k**). **l**, Schematic of AAV-DIO-mGLP1R (left) and AAV-DIO-hGLP1R (right) delivery in the CeA of *Glp1r-Cre;tdTomato* mice. h prefix denotes human; m prefix denotes mouse. **m**,**n**, Representative CeA images from **l** after treatment with vehicle (**m**) or danuglipron (**n**) (red, tdTomato; green, FOS; colocalization, white arrowheads). Scale bar, 100 µm. **o**, Quantification of FOS$^+$tdTomato$^+$ cells from **m**,**n** (Veh $n = 3$, Dan $n = 4$ per virus). **p**, Schematic of AAV-DIO-GCaMP7s plus AAV-DIO-mGLP1R or AAV-DIO-hGLP1R administration with fibre implant in the CeA of *Glp1r-Cre* mice. **q**,**r**, Heat maps of *z*-scored calcium signals during one hour of fibre photometry after treatment with vehicle or danuglipron in mGLP1R (**q**) or hGLP1R (**r**) mice ($n = 6$ per condition). **s**, Quantification of area under the curve (AUC) from **q**,**r**. **t**, Significant calcium event counts from **q**,**r**. **u**, Schematic of AAV-DIO-eYFP or AAV-DIO-ChR2-eYFP delivery with a fibre-optic implant in the CeA of *Glp1r-Cre* mice. **v**,**w**, Stimulation frequency response of one-hour SD (**v**) or HFD (**w**) intake in eYFP or ChR2 mice ($n = 5$ per group). **x**, Schematic of AAV-Cre (conditional *Glp1r* knockout) or AAV-GFP (control) delivery in the CeA of *Glp1r*$^{flox/flox}$ mice. **y**, Four-hour SD or HFD intake after treatment with liraglutide in GFP- or Cre-expressing mice (AAV-GFP $n = 11$, AAV-Cre $n = 12$). Data are mean ± s.e.m. Statistical tests: two-way ANOVA with Bonferroni correction (**b**–**k**,**t**,**v**,**w**); two-way ANOVA with Tukey's HSD correction (**o**); unpaired *t*-test (**s**); Welch's *t*-test (**y**). $^*P < 0.05$; $^{**}P < 0.01$; $^{***}P < 0.001$.

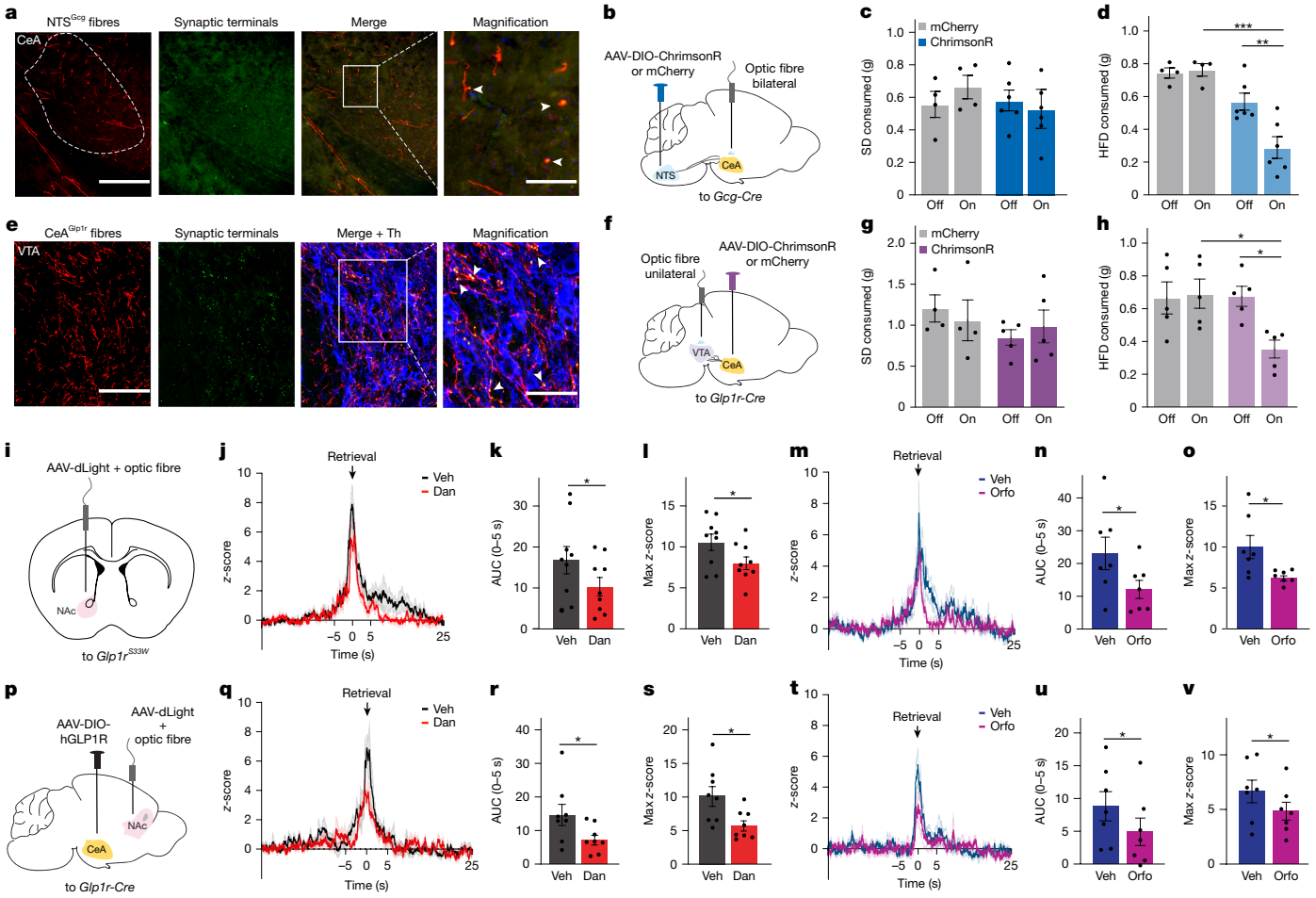

Fig. 5 | CeA^{Glp1r} neurons project to the VTA to modulate dopamine output to the NAc in response to HFD. **a**, Representative CeA image after NTS injection of AAV-DIO-mGFP-2A-Synaptophysin-mRuby in *Gcg-Cre* mice; fibres (red, pseudocoloured mGFP) and synaptic terminals (green, pseudocoloured mRuby). Magnified image highlights terminals (arrowheads). Scale bars, 200 µm (main) and 50 µm (magnified). **b**, Schematic of AAV-DIO-ChrimsonR or AAV-DIO-mCherry delivery in the NTS of *Gcg-Cre* mice with bilateral CeA fibre-optic implants. **c**,**d**, One-hour intake of SD (**c**) or HFD (**d**) in mCherry ($n = 4$) or ChrimsonR ($n = 6$) mice from **b** during optogenetic stimulation. **e**, Representative VTA image after CeA injection of AAV-DIO-mGFP-2A-Synaptophysin-mRuby in *Glp1r-Cre* mice; pseudocolouring scheme as in **a**, plus tyrosine hydroxylase (Th, blue). Magnified image highlights terminals (arrowheads). Scale bars, 100 µm (main) and 50 µm (magnified). **f**, Schematic of AAV-DIO-ChrimsonR or AAV-DIO-mCherry delivery in the CeA of *Glp1r-Cre* mice with a unilateral VTA fibre-optic implant. **g**,**h**, One-hour intake of SD (**g**) or HFD (**h**) in mCherry ($n = 4$) or ChrimsonR ($n = 5$) mice from **f** during optogenetic stimulation. **i**, Schematic of AAV-dLight1.3b delivery and NAc fibre implant in *Glp1r*^{S33W} mice. **j**–**l**, NAc dopamine responses to HFD after vehicle or danuglipron. **j**, Mean *z*-score traces aligned to food retrieval ($t = 0$), averaged across five trials per mouse. **k**, AUC. **l**, Maximum *z*-score within the retrieval window ($n = 9$). **m**–**o**, Same as **j**–**l** after vehicle or orforglipron: mean *z*-score traces (**m**), AUC (**n**) and maximum *z*-score (**o**) ($n = 7$). **p**, Schematic of AAV-dLight1.3b delivery and NAc fibre implant plus AAV-DIO-hGLP1R delivery in the CeA of *Glp1r-Cre* mice. **q**–**s**, NAc dopamine responses to HFD from mice in **p** after vehicle or danuglipron analysed as in **j**–**l**: mean *z*-score traces (**q**), AUC (**r**) and maximum *z*-score (**s**) ($n = 8$). **t**–**v**, Same as **q**–**s** after vehicle or orforglipron: mean *z*-score traces (**t**), AUC (**u**) and maximum *z*-score (**v**) ($n = 7$). All data are mean ± s.e.m. Statistical tests: two-way ANOVA with Tukey's HSD correction (**c**,**d**,**g**,**h**); paired *t*-test (**k**,**l**,**n**,**o**,**r**,**s**,**u**,**v**). $^*P < 0.05$; $^{**}P < 0.01$; $^{***}P < 0.001$.

Fig. 8). Optogenetic activation during one-hour feeding sessions reduced HFD consumption significantly without affecting SD intake (Fig. 4u–w), recapitulating the anorectic effects of danuglipron in CeA-hGLP1R mice (Fig. 4k and Extended Data Fig. 7b,c). To test whether CeA *Glp1r* is required for GLP1RA-mediated feeding suppression, we bilaterally injected AAV-Cre or AAV-GFP into the CeA of *Glp1r*$^{flox/flox}$ mice (Fig. 4x). Because *Glp1r*$^{flox/flox}$ mice lack the S33W mutation that is required for small-molecule sensitivity, we used the peptide agonist liraglutide, which activates WT GLP1R. Deletion of CeA *Glp1r* had no effect on SD intake, but significantly reduced the ability of liraglutide to inhibit HFD consumption (Fig. 4y and Supplementary Data Fig. 9). Because systemic liraglutide is unlikely to reach CeA^{Glp1r} neurons at high concentrations, CeA fibre photometry (Extended Data Fig. 8h–j) and FOS data[13,26,29,30] (Fig. 3d,h) support a model in which liraglutide acts through upstream GLP1R pathways but requires *Glp1r* in the CeA for full suppression of HFD intake. Together, these results establish CeA^{Glp1r} neurons as a crucial node in the circuit through which GLP1RAs suppress reward-driven feeding.

Small molecules modulate dopamine via the CeA

We next asked whether CeA^{Glp1r} neurons receive endogenous glucagon-like peptide 1 (GLP1) input. We selectively expressed fluorescently tagged synaptophysin in NTS^{Gcg} neurons, the most likely source of GLP1 in the central nervous system[43]. This allowed us to detect NTS^{Gcg} synaptic terminals in the CeA (Fig. 5a), indicating that CeA^{Glp1r} neurons are capable of receiving both GLP1 and other presynaptic input from NTS^{Gcg} neurons. To functionally confirm this connection, we Cre-dependently expressed ChrimsonR (a red-shifted optogenetic actuator) or mCherry in the NTS of *Gcg-Cre* mice and placed optic fibres bilaterally in their CeA (Fig. 5b). Stimulating CeA-projecting NTS^{Gcg} axon

terminals significantly inhibited HFD but not SD intake (Fig. 5c,d). These findings underscore that the CeA is a key integrative hub in which GLP1 signalling, both pharmacologically induced and naturally occurring, converges to curb hedonic feeding[44].

Having established that CeA^{Glp1r} activity selectively suppresses hedonic feeding, we next asked whether this amygdalar node feeds directly into the mesolimbic reward pathway, paralleling other GLP1R-based circuits that impinge on midbrain dopamine neurons[45,46]. Anatomical tracing from the CeA of *Glp1r-Cre* mice, using AAV-DIO-mGFP-2A-Synaptophysin-mRuby or AAV-DIO-ChR2-eYFP, revealed pronounced projections from CeA^{Glp1r} neurons to the ventral tegmental area (VTA) (Fig. 5e, Extended Data Fig. 9a,b and Supplementary Fig. 8). In complementary experiments, fluorescent marker expression from retroAAV-oNLS-oScarlet (a retrograde tracer) delivered into the VTA colocalized with Cre-dependent ChR2–eYFP expression in the CeA of *Glp1r-Cre* mice (Extended Data Fig. 9e–g) confirming direct CeA^{Glp1r}-to-VTA connectivity. Furthermore, monosynaptic rabies tracing of VTA dopamine cells labelled CeA^{Glp1r} neurons (Extended Data Fig. 9h–j), demonstrating that CeA^{Glp1r} neurons make synaptic connections with VTA dopamine neurons. Finally, to test functional relevance, we expressed Cre-dependent ChrimsonR or mCherry in CeA^{Glp1r} neurons and implanted an optic fibre in the VTA. Optogenetic stimulation of CeA axon terminals in the VTA selectively reduced HFD intake without affecting SD consumption (Fig. 5f–h), showing that CeA^{Glp1r}-to-VTA signalling is sufficient to inhibit hedonic feeding.

These findings support a model in which NTS^{Gcg}-driven activation of GABAergic CeA^{Glp1r} neurons suppresses VTA dopamine output and thereby blunts accumbal dopamine release during hedonic feeding. To test this, we virally expressed the genetically encoded fluorescent dopamine sensor dLight1.3b in the nucleus accumbens (NAc) of *Glp1r*^{S33W} mice and recorded dopamine transients in response to HFD consumption after administration of liraglutide, danuglipron or orforglipron (Fig. 5i). All three GLP1RAs significantly attenuated both the peak and the consumption-associated dopamine signals, demonstrating that this is a general property of GLP1R activation rather than being compound specific (Fig. 5j–o and Extended Data Fig. 10a–d). By contrast, danuglipron had no effect on HFD-evoked dopamine release in WT mice (Extended Data Fig. 10e–h), confirming that these small molecules require the humanized receptor to dampen reward-related dopamine signalling. To establish a causal link between CeA^{Glp1r} neuron activity and mesolimbic dopamine output, we selectively expressed human GLP1R in the CeA of *Glp1r-Cre* mice and monitored NAc dopamine dynamics during HFD consumption after administration of danuglipron or orforglipron (Fig. 5p and Extended Data Fig. 10i–k). Notably, both small-molecule treatments markedly blunted the peak and consumption-associated dopamine transients (Fig. 5q–v), indicating that the activation of CeA^{Glp1r} neurons suppresses reward-driven dopamine signalling. By showing that this CeA→VTA→NAc pathway operates alongside previously characterized hindbrain→midbrain GLP1R circuits[46–48], our results reveal a distributed network of GLP1R-expressing neurons that orchestrates the suppression of food consumption[15–18,49].

Discussion

Our data uncover a previously uncharacterized amygdalar pathway through which next-generation GLP1R agonists modulate reward-driven feeding. Specifically, CeA^{Glp1r} neurons are well-positioned to receive endogenous and exogenous GLP1 input and modulate VTA activity, thereby linking metabolic signals to dopamine-dependent reward circuits[3,46–49]. Consistent with this role, our experiments show that activating CeA^{Glp1r} neurons preferentially suppresses palatable food consumption, supporting a broad role for the CeA in encoding food valence rather than a global hunger or satiety state. This circuit complements established hindbrain to midbrain GLP1R pathways and helps explain how GLP1R agonists influence not only energy balance but also motivated behaviours[10,11,46–49]. More broadly, our findings suggest that GLP1R agonists could have applications in disorders of dysregulated reward signalling, including substance-use disorders. As small-molecule compounds such as orforglipron—hailed as "a product for the masses"[50]—move swiftly towards widespread clinical use[5,6,20], it will be crucial to define their long-term effects on mesolimbic circuitry and motivated behaviours.

Online content

Any methods, additional references, Nature Portfolio reporting summaries, source data, extended data, supplementary information, acknowledgements, peer review information; details of author contributions and competing interests; and statements of data and code availability are available at https://doi.org/10.1038/s41586-026-10444-4.

1. Wilding, J. P. H. et al. Once-weekly semaglutide in adults with overweight or obesity. *N. Engl. J. Med.* **384**, 989–1002 (2021).
2. Drucker, D. J. Mechanisms of action and therapeutic application of glucagon-like peptide-1. *Cell Metab.* **27**, 740–756 (2018).
3. Drucker, D. J. The benefits of GLP-1 drugs beyond obesity. *Science* **385**, 258–260 (2024).
4. Luna Ceron, E. et al. Current Insights, advantages and challenges of small molecule glucagon-like peptide 1 receptor agonists: a scoping review. *J. Brown Hosp. Med.* **4**, 19–32 (2025).
5. Wharton, S. et al. Daily oral GLP-1 receptor agonist orforglipron for adults with obesity. *N. Engl. J. Med.* **389**, 877–888 (2023).
6. Dutta, D. et al. Orforglipron, a novel non-peptide oral daily glucagon-like peptide-1 receptor agonist as an anti-obesity medicine: a systematic review and meta-analysis. *Obes. Sci. Pract.* **10**, e743 (2024).
7. Saxena, A. R. et al. Danuglipron (PF-06882961) in type 2 diabetes: a randomized, placebo-controlled, multiple ascending-dose phase 1 trial. *Nat. Med.* **27**, 1079–1087 (2021).
8. Griffith, D. A. et al. A small-molecule oral agonist of the human glucagon-like peptide-1 receptor. *J. Med. Chem.* **65**, 8208–8226 (2022).
9. Zhang, X. et al. Differential GLP-1R binding and activation by peptide and non-peptide agonists. *Mol. Cell* **80**, 485–500 (2020).
10. Wang, W. et al. Associations of semaglutide with incidence and recurrence of alcohol use disorder in real-world population. *Nat. Commun.* **15**, 4548 (2024).
11. Wang, W. et al. Association of semaglutide with reduced incidence and relapse of cannabis use disorder in real-world populations: a retrospective cohort study. *Mol. Psychiatry* **29**, 2587–2598 (2024).
12. Baggio, L. L. & Drucker, D. J. Glucagon-like peptide-1 receptors in the brain: controlling food intake and body weight. *J. Clin. Invest.* **124**, 4223–4226 (2014).
13. Salinas, C. B. G. et al. Integrated brain atlas for unbiased mapping of nervous system effects following liraglutide treatment. *Sci. Rep.* **8**, 10310 (2018).
14. Secher, A. et al. The arcuate nucleus mediates GLP-1 receptor agonist liraglutide-dependent weight loss. *J. Clin. Invest.* **124**, 4473–4488 (2014).
15. Huang, K.-P. et al. Dissociable hindbrain GLP1R circuits for satiety and aversion. *Nature* **632**, 585–593 (2024).
16. Kim, K. S. et al. GLP-1 increases preingestive satiation via hypothalamic circuits in mice and humans. *Science* **385**, 438–446 (2024).
17. Webster, A. N. et al. Molecular connectomics reveals a glucagon-like peptide 1-sensitive neural circuit for satiety. *Nat. Metab.* **6**, 2354–2373 (2024).
18. Sisley, S. et al. Neuronal GLP1R mediates liraglutide's anorectic but not glucose-lowering effect. *J. Clin. Invest.* **124**, 2456–2463 (2014).
19. Kawai, T. et al. Structural basis for GLP-1 receptor activation by LY3502970, an orally active nonpeptide agonist. *Proc. Natl Acad. Sci. USA* **117**, 29959–29967 (2020).
20. Sloop, K. W. et al. The pharmacological basis for nonpeptide agonism of the GLP-1 receptor by orforglipron. *Sci. Transl. Med.* **16**, eadp5765 (2024).
21. Sonne, N. et al. Generation and characterisation of a humanised GLP-1 receptor mouse model for translational drug development. *EBioMedicine* **124**, 106121 (2026).
22. Grippo, R. M. et al. Dopamine signaling in the suprachiasmatic nucleus enables weight gain associated with hedonic feeding. *Curr. Biol.* **30**, 196–208 (2020).
23. Liu, C. M. & Kanoski, S. E. Homeostatic and non-homeostatic controls of feeding behavior: Distinct vs. common neural systems. *Physiol. Behav.* **193**, 223–231 (2018).
24. Pereira, T. D. et al. SLEAP: A deep learning system for multi-animal pose tracking. *Nat. Methods* **19**, 486–495 (2022).
25. Weinreb, C. et al. Keypoint-MoSeq: parsing behavior by linking point tracking to pose dynamics. *Nat. Methods* **21**, 1329–1339 (2024).
26. Gabery, S. et al. Semaglutide lowers body weight in rodents via distributed neural pathways. *JCI Insight* **5**, e133429 (2020).
27. Alhadeff, A. L. et al. Endogenous glucagon-like peptide-1 receptor signaling in the nucleus tractus solitarius is required for food intake control. *Neuropsychopharmacology* **42**, 1471–1479 (2017).
28. Zeng, N. et al. Anatomical and functional characterization of central amygdala glucagon-like peptide 1 receptor expressing neurons. *Front. Behav. Neurosci.* **15**, 724030 (2021).
29. Hansen, H. H. et al. Whole-brain activation signatures of weight-lowering drugs. *Mol. Metab.* **47**, 101171 (2021).
30. Petersen, J. et al. GLP-1-directed NMDA receptor antagonism for obesity treatment. *Nature* **629**, 1133–1141 (2024).

31. Zhang, C. et al. Area postrema cell types that mediate nausea-associated behaviors. *Neuron* **109**, 461–472 (2021).
32. Lean, M. E. J. et al. Tolerability of nausea and vomiting and associations with weight loss in a randomized trial of liraglutide in obese, non-diabetic adults. *Int. J. Obes.* **38**, 689–697 (2014).
33. Izadi, M. S. & Radahmadi, M. Overview of the central amygdala role in feeding behaviour. *Br. J. Nutr.* **127**, 953–960 (2022).
34. Fermani, F. et al. Food and water intake are regulated by distinct central amygdala circuits revealed using intersectional genetics. *Nat. Commun.* **16**, 3072 (2025).
35. Cai, H., Haubensak, W., Anthony, T. E. & Anderson, D. J. Central amygdala PKC-δ^{+} neurons mediate the influence of multiple anorexigenic signals. *Nat. Neurosci.* **17**, 1240–1248 (2014).
36. Douglass, A. M. et al. Central amygdala circuits modulate food consumption through a positive-valence mechanism. *Nat. Neurosci.* **20**, 1384–1394 (2017).
37. Hardaway, J. A. et al. Central amygdala preprononociceptin-expressing neurons mediate palatable food consumption and reward. *Neuron* **102**, 1037–1052 (2019).
38. Duran, M. et al. Integration of glucagon-like peptide 1 receptor actions through the central amygdala. *Endocrinology* **166**, bqaf019 (2025).
39. Peters, C. et al. Transcriptomics reveals amygdala neuron regulation by fasting and ghrelin thereby promoting feeding. *Sci. Adv.* **9**, eadf6521 (2023).
40. Zhang, M. et al. Molecularly defined and spatially resolved cell atlas of the whole mouse brain. *Nature* **624**, 343–354 (2023).
41. Zheng, Z. et al. Glucagon-like peptide-1 receptor: mechanisms and advances in therapy. *Signal Transduct. Target. Ther.* **9**, 234 (2024).
42. Zhang, H. et al. Binding sites and design strategies for small molecule GLP-1R agonists. *Eur. J. Med. Chem.* **275**, 116632 (2024).
43. Larsen, P. J., Tang-Christensen, M., Holst, J. J. & Ørskov, C. Distribution of glucagon-like peptide-1 and other preproglucagon-derived peptides in the rat hypothalamus and brainstem. *Neuroscience* **77**, 257–270 (1997).
44. Wang, H. et al. Parallel gut-to-brain pathways orchestrate feeding behaviors. *Nat. Neurosci.* **28**, 320–335 (2025).
45. Wang, X.-F. et al. Endogenous glucagon-like peptide-1 suppresses high-fat food intake by reducing synaptic drive onto mesolimbic dopamine neurons. *Cell Rep.* **12**, 726–733 (2015).
46. Alhadeff, A. L., Rupprecht, L. E. & Hayes, M. R. GLP-1 neurons in the nucleus of the solitary tract project directly to the ventral tegmental area and nucleus accumbens to control for food intake. *Endocrinology* **153**, 647–658 (2012).
47. Merkel, R. et al. An endogenous GLP-1 circuit engages VTA GABA neurons to regulate mesolimbic dopamine neurons and attenuate cocaine seeking. *Sci. Adv.* **11**, eadr5051 (2025).
48. Alhadeff, A. L. & Grill, H. J. Hindbrain nucleus tractus solitarius glucagon-like peptide-1 receptor signaling reduces appetitive and motivational aspects of feeding. *Am. J. Physiol. Regul. Integr. Comp. Physiol.* **307**, R465–R470 (2014).
49. Fortin, S. M. & Roitman, M. F. Central GLP-1 receptor activation modulates cocaine-evoked phasic dopamine signaling in the nucleus accumbens core. *Physiol. Behav.* **176**, 17–25 (2017).
50. Dave Ricks, CEO of Eli Lilly | the All-In interview. *All-In Podcast* (2024); https://youtu.be/023exhA9irY?si=zvw1aQ6cVXtNlfy5&t=2181.
51. Claudi, F. Mouse top detailed. *Zenodo* https://doi.org/10.5281/zenodo.3925997 (2020).

Methods

Mouse lines

All experiments were conducted in compliance with the Association for Assessment of Laboratory Animal Care policies and approved by the Institutional Animal Care and Use Committees of the University of Virginia, University of Washington and University of California, Irvine. Mice were housed on a 12-h:12-h light–dark (LD) cycle with food (PicoLab Rodent Diet 5053) and water provided ad libitum unless otherwise indicated. For experiments, we used 8-week or older male and female C57BL/6J mice, *Glp1r-IRES-Cre* mice (Glp1rtm1.1(cre)Lbrl/RcngJ, strain 029283, RRID: IMSR_JAX:029283), *Glp1r-IRES-Cre* mice crossed to the Ai14 tdTomato reporter line (B6.Cg-Gt(ROSA)26Sortm14(CAG-tdTomato)Hze/J, strain 007914, RRID: IMSR_JAX:007914), *Glp1r*$^{flox/flox}$ mice (B6(SJL)-Glp1rtm1.1Stof/J, strain 035238, RRID: IMSR_JAX:035238), *Dat-Cre* mice (B6.SJL-Slc6a3tm1.1(cre)Bkmn/J, strain 006660, RRID: IMSR_JAX:006660) *Gcg-Cre* mice (C57BL/6J-Tg(Gcg-cre)-1Mmsc/Mmmh, stock 051056-MU, RRID: MMRRC_051056-MU) and *Glp1r*^{S33W} mice (described below). *Gcg-Cre* mice were rederived by in vitro fertilization from frozen sperm (MMRRC, 051056-MU). Approximately equal numbers of males and females were used per group unless otherwise specified.

Generation of *Glp1r*^{S33W} mice

The *Glp1r*^{S33W} mouse line was generated by CRISPR–Cas9 homologous repair at the University of Virginia Genetically Engineered Murine Model Core. In brief, Cas9 (Alt-R S.p. Cas9 Nuclease V3, 100 µg, 1081058), Alt-R HDR Donor Oligo repair template (see subsection below), tracrRNA (Alt-R CRISPR–Cas9 tracrRNA, 5 nmol, 1072532) and CRISPR–Cas9 crRNA XT (ATTTCTGCACCGTCTCTGAG) were microinjected into a fertilized B6SJL zygote and implanted into a pseudopregnant female. Founder pups were genotyped as described below and backcrossed to C57BL/6J mice for at least four generations before experimentation. This strain will be available at The Jackson Laboratory Repository with the JAX 040551 *Glp1r*^{S33W} mouse line.

Repair template. aagagggtgggagtccagtgggaccagaggggctgctggagc cacggggcttctgcttttatttctgctttcccttgtagGGTACCACGGTG**TCGCTCTGG GAAACCGTCCAAAAGTGG**AGAGAATACCGGCGGCAGTGCCAGCGTTT CCTCACGGAAGCGCCACTCCTGGCCACAGgtgcgtccagatgaggcctcacg. Lowercase: non-coding regions; uppercase: coding regions; bold: mutated region; underline: codon coding for S33W mutation.

Validation of Glp1r^{S33W} mice

Tail snips were obtained from pups at 3 weeks of age. DNA was extracted with an extraction buffer (Sigma, E7526) and tissue prep solution (Sigma, T3073), heated for 10 min and 3 min at 55 °C and 100 °C, respectively, then neutralized with a neutralization solution (Sigma, N3910). PrimeSTAR High Fidelity PCR (Takara, R050A) was performed with 1 µl cDNA and 10 µM 5′–3′ F (GATCCCCAAAGTG GCAGTCA) and 5′–3′ R (AGCTATGGACTGGGGATCGT) primers. After amplification, the PCR product was run on a 1.2% agarose gel and bands were cut out at 330 bp. DNA was gel-extracted and purified (QIAGEN, 28704), mixed with 5 µM right primer, H_2O, and subsequently sent to be analysed by Sanger sequencing (Azenta). Chromatogram results were analysed to assign WT, heterozygous or homozygous genotypes for each mouse.

Generation of GLP1R viruses

The full-length human *GLP1R* gene was obtained by PCR, amplifying the human fragment from GLP1R-Tango (plasmid from Addgene, 66295, RRID: Addgene_66295), including the leader sequence present in the GLP1R-Tango. The primers used were: 5′–3′ F (AAA GCTAGCGCCACCATGAAGACGATCATCGCCCTGAGC) and 5′–3′ R (TTTGGCGCGCCCTAA-GAGCAGGACGCCTGACAAGT), ligating the product into pAAV-hSyn-DIO-EGFP (plasmid from Addgene, 50457, RRID: Addgene_50457) in place of the EGFP in NheI and AscI sites to produce the human GLP1R virus construct (AAV-hSyn-DIO-hGLP1R). The full-length mouse *Glp1r* WT gene was synthesized by Twist Biosciences, generating an NheI and an AscI fragment. This construct included the same leader sequence present in the human construct, as well as an HA tag encoded at the C terminus of the full-length mouse protein-coding region. The fragment was inserted into pAAV-hSyn-DIO-EGFP (plasmid from Addgene, 50457, RRID: Addgene_50457) in place of EGFP to produce the plasmid construct (AAV-hSyn-DIO-mGLP1R-HA). The full-length mouse *Glp1r* gene bearing a Ser-to-Trp mutation at position 33 (S33W) was made by inserting a synthetic NheI and StuI fragment prepared by Twist Biosciences, containing the single mutation within this fragment. This was cloned into the sites present in the WT construct to produce the S33W mouse mutant, followed by an HA tag encoded at the C terminus (AAV-hSyn-DIO-mGLP1R^{S33W}-HA). Viral plasmid constructs were confirmed by Sanger sequencing. Virus plasmid constructs were prepared and sent to the University of North Carolina Viral Core for preparation of the AAV (serotype 8). In experiments using AAV-DIO-hGLP1R, AAV-DIO-mGlp1r-HA and AAV-DIO-mGLP1R^{S33W}-HA to drive receptor expression, viral titres were carefully calibrated to approximate endogenous receptor levels (Supplementary Fig. 5b); nonetheless, this overexpression approach might alter receptor distribution or signalling, and constitutes a limitation of the model.

Stereotaxic surgery

Mice were anaesthetized with isoflurane (5% induction and 2–2.5% maintenance; Isothesia) and placed in a stereotaxic apparatus (AWD). A heating pad was used throughout the surgery to maintain body temperature, and ocular lubricant was applied to the eyes to prevent desiccation. A total of 200–400 nl virus (rAAV8/AAV2-hSyn-DIO-hGLP1R, plasmid from Addgene, virus packaged at UNC GTC Vector Core, AV9862 (100 µl at titre ≥ 1.5×10^{13} vg ml^{-1}); AAV8-hSyn-DIO-mGLP1R^{S33W}-HA, synthesized by Twist Biosciences, virus packaged at UNC GTC Vector Core, AV10104 (100 µl at titre ≥ 8.2×10^{12} vg ml^{-1}); AAV8-hSyn-DIO-mGLP1R-HA, synthesized by Twist Biosciences, virus packaged at UNC GTC Vector Core, AV10103 (100 µl at titre ≥ 4.5×10^{12} vg ml^{-1}); pAAV9-syn-dLight1.3b, plasmid from Addgene, 135762, RRID: Addgene_135762, virus packaged at UNC GTC Vector Core (100 µl at titre ≥ 1.5×10^{13} vg ml^{-1}); pAAV1-EF1a-DIO- hChR2(H134R)-EYFP-WPRE-HGHpA, plasmid from Addgene, 20298, RRID: Addgene_20298, virus packaged at UNC GTC Vector Core (100 µl at titre ≥ 7×10^{12} vg ml^{-1}); pGP-AAV1-syn-DIO-jGCaMP7s-WPRE, plasmid from Addgene, 104491, RRID: Addgene_104491, virus packaged at UNC GTC Vector Core (100 µl at titre ≥ 1×10^{13} vg ml^{-1}); pAAV1-Ef1a-DIO-EYFP, plasmid from Addgene, 27056, RRID: Addgene_27056, virus packaged at UNC GTC Vector Core (100 µl at titre ≥ 1×10^{13} vg ml^{-1}); AAV8-hSyn-DIO-mCherry, plasmid from Addgene 50459, RRID: Addgene_50459, virus packaged at UNC Vector Core (100 µl at titre ≥ 7×10^{12} vg ml^{-1}); pAAV-hSyn-FLEx-mGFP-2A-Synaptophysin-mRuby, plasmid from Addgene, 71760, RRID: Addgene_71760, virus packaged at UNC Vector Core; pENN.AAV.hSyn.HI.eGFP-Cre.WPRE.SV40, plasmid from Addgene, 105540-AAV8, RRID: Addgene_105540-AAV8, virus packaged at UNC Vector Core (100 µl at titre ≥ 1×10^{13} vg ml^{-1}); pAAV-hSyn-DIO-ChrimsonR-mRuby2-ST, plasmid from Addgene, 105448, RRID: Addgene_105448-AAV9, virus packaged at UNC Vector Core (100 µl at titre ≥ 1×10^{13} vg ml^{-1}); pAAV-hSyn-EGFP, plasmid from Addgene, 50465-AAV8, RRID: Addgene_50465-AAV8, virus packaged at UNC Vector Core (100 µl at titre ≥ 7×10^{12} vg ml^{-1}), retroAAV2-EF1a-oNLS-oScarlet[52] (100 µl at titre ≥ 3×10^{13} vg ml^{-1})), was delivered using a glass pipette at a flow rate of 50 nl per min driven by a microsyringe pump controller (World Precision Instruments, model Micro 4) per targeted site. The syringe needle was left in place for 10 min and was completely withdrawn 17 min after viral delivery. For in vivo calcium and dopamine imaging and optogenetics, a unilateral fibre-optic cannula (RWD, Ceramic Ferrule, Ø 400 µm, 0.5 numerical

aperture) was implanted 0.2 mm dorsal to the viral injection coordinates after viral delivery and stabilized on the skull with dental cement (C&B Metabond, Parkell). A minimum of 3 weeks was allowed for recovery and transgene expression after surgery. Stereotaxic coordinates relative to Bregma (G. Paxinos and K. B. J. Franklin): BMH (encompassing the DMH, arcuate nucleus, median eminence and ventromedial hypothalamus), mediolateral (ML): ±0.3 mm, anterior–posterior (AP): −1.4 mm, dorsoventral (DV): −5.9 mm; DMH, ML: ±0.3 mm, AP: −1.8 mm, DV: −5.4 mm; CeA, ML: ±2.7 mm, AP: −1.3 mm, DV: −4.6 mm; VTA, ML: ±0.5 mm, AP: −3.6 mm, DV: −4.5 mm; NAc, ML: ±1.25 mm, AP: +1.0 mm, DV: −4.7 mm from Bregma; and NTS–AP, ML: ±0.15 mm, AP: −0.3 mm, DV: −0.1, −0.4 mm from the zero point of the calamus scriptorius.

For rabies tracing, a total of 500 nl, containing a 1:1 mixture of AAV5-FLEx^{loxP}-TC (UNC Vector Core, titre ≥ 2.4×10^{12} gc ml^{-1}) and AAV8-FLEx^{loxP}-RABV-G (UNC Vector Core, titre ≥ 1.0 × 10^{12} gc ml^{-1}), was injected into the VTA of *DAT-Cre* mice. Fourteen days later, 500 nl of G-deleted, GFP-expressing, EnvA-pseudotyped rabies virus (RABVΔG-H2B-GFP-EnvA (generated at UC Irvine, K.T.B. laboratory, titre ≥ 5 × 10^8 colony forming units per ml)) was injected into the same site. Five days after the rabies virus injection, brains were collected for further processing. All surgical procedures were performed under sterile conditions and in accordance with the guidelines of the University of Virginia Institutional Animal Care and Use Committee. Histological analysis was performed to validate the success of intracranial surgeries. Mice with unsuccessful viral or implant targeting were excluded from the analysis.

GLP1R agonists

Liraglutide powder (Selleck, S8256) was dissolved in 0.9% NaCl sterile saline, lightly sonicated and further diluted in 0.9% NaCl sterile saline to 0.03 mg ml^{-1}. Danuglipron powder (Selleck, S9851) was dissolved to 30 mg ml^{-1} in 100% ethanol with gentle sonication, then diluted to 3 mg ml^{-1} (food intake) or 0.3 mg ml^{-1} (GTT) in vehicle (1 M NaOH, 2% Tween 80, 5% polyethylene glycol (PEG) 400, 5% dextrose)[7]. Orforglipron powder (MedChemExpress, HY-112185) was dissolved to 10 mg ml^{-1} in dimethyl sulfoxide and further diluted in 0.9% NaCl sterile saline to 0.1 mg ml^{-1}. The dosage for danuglipron and orforglipron was decided on the basis of previous literature.

Histological analysis and imaging

For fixed tissue collection, mice were deeply anaesthetized (ketamine:xylazine, 280:80 mg kg^{-1}, intraperitoneally) and perfused intracardially with ice-cold 0.01 M phosphate buffer solution (PBS), followed by fixative solution (4% paraformaldehyde in PBS at a pH of 7.4). For testing brain region FOS activation (Fig. 3), vehicle (control), danuglipron (30 mg kg^{-1}), orforglipron (1 mg kg^{-1}) or liraglutide (0.3 mg kg^{-1}) was delivered by intraperitoneal injection or oral gavage 2 hours (or 6 hours for orforglipron) before perfusion and brain collection. After perfusion, brains were collected and post-fixed overnight at 4 °C in paraformaldehyde. Fixed brains were then transferred into 30% sucrose in PBS for 24 h and then frozen on dry ice. Frozen brains were sectioned immediately or stored at −80 °C for future processing. Coronal sections (30 µm) were collected with a cryostat (Microm HM 505 E). Sections were permeabilized with 0.3% Triton X-100 in PBS (PBS-T) and blocked with 3% normal donkey serum (Jackson ImmunoResearch, RRID: AB_2337258) in PBS-T (PBS-T DS) for 30 min at room temperature. Sections were then incubated overnight at room temperature in primary antibodies diluted in PBS-T DS. For visualization, sections were washed with PBS-T and incubated with appropriate secondary antibodies diluted in PBS-T DS for 2 hours at room temperature. Sections were washed three times with PBS and mounted using DAPI Fluoromount-G (Southern Biotech, 0100-20). Images were captured on a Zeiss Axioplan 2 Imaging microscope equipped with an AxioCam MRm camera using AxioVision 4.6 software (Zeiss), or confocal microscope imaging was performed on a Zeiss LSM 800 microscope. The following primary antibodies were used for fluorescent labelling: anti-c-FOS (rabbit, 1:1,000; Synaptic Systems, 226003, RRID: AB_2231974), anti-DsRed (rabbit, 1:1,000; Takara Bio, 632496, RRID: AB_10013483), anti-tdTomato (goat, 1:1,000; Arigobio, ARG55724), anti-human GLP1R (rabbit, 1:200; Invitrogen, PA5-97789, RRID: AB_2812404), anti-HA (rabbit, 1:1,000, Cell Signaling, 3724), anti-Th (rabbit, 1:500; Chemicon, AB152) and anti-GFP (goat, 1:500; Rockland, 600-101-215). The secondary antibodies (Jackson ImmunoResearch) used were Cy2-conjugated donkey anti-rabbit (1:250; 711-225-152, RRID: AB_2340612), Cy3-conjugated donkey anti-rabbit (1:250; 711-165-152, RRID: AB_2307443), Cy5-conjugated donkey anti-rabbit (1:250; 711-175-152, RRID: AB_2340607), Cy3-conjugated donkey anti-goat (1:250; 705-165-147, RRID: AB_2307351) and Alexa-Fluor 488 donkey anti-goat (1:250; 705-545-003, RRID: AB_2340428). RNA fluorescent in situ hybridization was performed on fixed brain slices with a probe to detect *Glp1r* RNA (RNAscope Multiplex Fluorescent Reagent Kit v2 Assay, Advanced Cell Diagnostics, 1297311, 24065D). All procedures were performed according to the manufacturer's instructions.

Antigen retrieval for human GLP1R staining

Antigen retrieval was performed before immunohistochemistry staining of human GLP1R, by incubating the sections in the following solutions sequentially in room temperature: 1% NaOH + 0.3% H_2O_2 in PBS for 20 min, 0.3% glycine in PBS for 10 min and 0.03% sodium dodecyl sulfate in PBS for 10 min. Then, antigen-retrieval-treated sections were stained following the immunohistochemistry staining procedures described.

FOS analysis pipeline

FOS images were uploaded to ImageJ (Fiji) and cropped on the basis of brain regions outlined in the Allen Brain Atlas. The areas of the cropped regions were measured and recorded. Image thresholds were set per image and particles were analysed within the size restriction of 50–500 pixels. FOS particles were analysed per image, and total particles of each image were divided by total area of the image. At least three FOS images per region for each mouse were quantified and averaged per mouse and per genotype (WT or *Glp1r*^{S33W}). Ratios of NTS-to-AP FOS activation in *Glp1r*^{S33W} mice were calculated by dividing FOS per unit area of NTS by FOS per unit area of AP for each mouse, and averaged per injection. The heat map was generated by first normalizing each condition to WT control by region and clustered by column.

Single-nucleus RNA sequencing analysis

Using a previously published single-nucleus RNA sequencing atlas[39], we calculated the number of *Glp1r*$^+$ cells and other markers of interest and quantified their overlap, defining positive cells as those with mRNA counts greater than 0.

Metabolic analysis in the comprehensive laboratory animal monitoring system

Indirect calorimetry in the comprehensive laboratory animal monitoring system (CLAMS, Columbus Instruments) was used to evaluate metabolic parameters of WT and *Glp1r*^{S33W} mice. All WT and *Glp1r*^{S33W} mice were single-housed and maintained on a 12:12-h LD cycle with ad libitum access to food (PicoLab Rodent Diet 5053) and water. Metabolic measures of respiratory exchange ratio and energy expenditure were averaged over 3 days per mouse and per genotype (n = 10 or 11 mice per genotype). Averaged LD cycle and total 24-h respiratory exchange ratio and energy expenditure were analysed per genotype and per sex.

GTTs

WT or *Glp1r*^{S33W} mice were fasted for 16 h overnight before the start of the experiment (ZT10–ZT2). Mice received a tail snip and blood glucose measure using a glucometer (OneTouch Ultra Test Strips for Diabetes), along with injection or oral gavage of danuglipron (3 mg kg^{-1}) or liraglutide (0.3 mg kg^{-1}) 15 min before dextrose (D-glucose) injection,

or orforglipron (1 mg kg^{-1}) 240 min before dextrose. Orforglipron was intentionally administered 4 hours earlier because of its partial agonist properties, which mean that it takes longer for it to act. At time point 0, mice received a blood glucose measure and injection of dextrose (1 g kg^{-1}). At 15, 30, 60, 90 and 120 min after injection, blood glucose levels were measured.

Homeostatic (SD) food intake

Home cages were changed and food was removed from the home cage 1 hour before the start of the experiment. Mice were injected with vehicle or drug (danuglipron 30 mg kg^{-1}, liraglutide 0.3 mg kg^{-1} or orforglipron 1 mg kg^{-1}) at ZT11.5 (ZT8 for orforglipron), and two pellets of SD (PicoLab Rodent Diet 5053) were placed on the home-cage floor at ZT12. All experiments were done in light-tight boxes equipped with programmable lighting, allowing dark-cycle conditions to be maintained during the daytime without exposing the mice to ambient light. Food intake measurements were taken at 1, 2 and 4 hours after ZT12 using infrared night vision goggles (Nightfox Swift Night Vision Goggles). For the danuglipron dose–response experiment, 3 mg kg^{-1}, 10 mg kg^{-1} or 30 mg kg^{-1} danuglipron was injected at ZT12 and SD intake was measured two hours later. For post-fast refeeding experiments (Extended Data Fig. 1l–q), mice got new bedding and 16 h of food deprivation (ZT10–ZT2) followed by an injection of drug or vehicle injection at ZT2 and refeeding with SD (30 min after injection for danuglipron and liraglutide; 4 hours after injection for orforglipron). For all food intake measurements, except Fig. 4v,w and the panels in Fig. 5, values were rounded to the nearest 0.1 g; otherwise, data were not rounded.

Hedonic (HFD) food intake

Mice were habituated to HFD (Open Source, D12451; 4.73 kcal g^{-1}; 45% fat, 20% protein, 35% carbohydrate; 17% sucrose) for 1 hour over 2 days before testing days. SD was removed from the home cage 1 hour before the start of the experiment. Mice were injected with vehicle or drug (danuglipron 30 mg kg^{-1}, liraglutide 0.3 mg kg^{-1} or orforglipron 1 mg kg^{-1}) at ZT1.5 and one pellet of HFD was placed on the home-cage floor at ZT2 (ZT5.5 for orforglipron). Food intake measurements were taken at 1, 2 and 4 hours after HFD delivery. The same parameters were used in oral gavage experiments with danuglipron and orforglipron. All feeding experiments in Fig. 4a–k used a within-individual paired design. Within each viral cohort, the same mice received vehicle and danuglipron on separate, counterbalanced test days. The reported *n* values therefore correspond to paired vehicle and drug datasets for each mouse, and the plotted intake values reflect one test session per condition per mouse, averaged across mice.

Optogenetic food intake

For CeA^{Glp1r} soma stimulation, mice were single-housed for at least 5 days and habituated daily for 1 hour to a patch-cord and for 1 hour to HFD pellets over 2 consecutive days before testing for the hedonic feeding paradigm. On subsequent testing days, mice underwent optogenetic stimulation at frequencies of 0 Hz (control), 5 Hz, 10 Hz and 20 Hz for 1 hour each, which took place on separate days. For homeostatic feeding assessment using SD, mice were fasted overnight, whereas for hedonic feeding assessment (HFD), mice had ad libitum access to standard chow before testing. Food intake was quantified manually by weighing pre-measured SD or HFD pellets at the beginning and at the end of each 1-hour stimulation session. The laser stimulation protocol consisted of 473-nm blue light delivered at 20 Hz in a 1 s on, 3 s off pulse pattern. Light power exiting the fibre-optic cable was measured using an optical power meter (Thorlabs) and maintained at 8–10 mW across all experiments. All experiments were performed during the light phase, between ZT3 and ZT4. Mice with missed virus injections or off-target fibre placements were excluded from the analysis.

For axon-stimulation experiments, mice expressing ChrimsonR or mCherry in either NTS^{Gcg} terminals in the CeA or CeA^{Glp1r} terminals in the VTA were single-housed for at least 5 days and habituated daily for 1 hour to a patch-cord and for 1 hour to HFD pellets over 2 consecutive days before testing for the hedonic feeding paradigm. On different days, mice received 1-hour light stimulation at 0 Hz (control), 20 Hz (CeA^{Glp1r} axons) or 40 Hz (NTS^{Gcg} axons) with a 1 s on, 3 s off pulse pattern. Simulations were bilateral for NTS^{Gcg} axons in the CeA and unilateral for CeA^{Glp1r} axons in the VTA. Light power exiting the fibre-optic cable was measured using an optical power meter (Thorlabs) and maintained at 8–10 mW across all experiments. Homeostatic and hedonic feeding paradigms were assessed as explained above. All sessions were done during the light phase (ZT3–ZT4), and any mouse with mistargeted viral expression or fibre placement was excluded from analysis.

Weight-loss experiment

Male *Glp1r*^{S33W} mice (at least 8 weeks old) were placed on a HFD (Open Source, D12451; 4.73 kcal g^{-1}; 45% fat, 20% protein, 35% carbohydrates; 17% sucrose) for at least 8 weeks before the start of the experiment. Mice that did not gain at least 20% of their baseline body weight were excluded from testing, disqualifying female mice from this study. Male mice were randomly assigned to 21 days of vehicle or orforglipron (1 mg kg^{-1}) injection and were retested with the opposite treatment after 10 days of rest. *Glp1r*^{S33W} mice were injected daily at ZT6 and food and body weight were measured.

Conditioned taste avoidance

Mice were water deprived from ZT9 to ZT2 the next day and habituated to two water bottles for 2 days. Measurements of water bottles were taken from ZT2 to ZT3 to ensure mice were drinking. On the third day, mice got two 0.15% saccharin (98+%, Thermo Fisher Scientific Chemicals, 149001000) bottles for 1 hour and were immediately injected or orally gavaged with vehicle or drug (LiCl (125 mg kg^{-1}), danuglipron (30 mg kg^{-1}), liraglutide (0.3 mg kg^{-1}) or orforglipron (1 mg kg^{-1})). Normal water bottles were restored for the next 2 days. Water was again deprived at ZT9, and at ZT2 the next day, one water bottle and one 0.15% saccharin bottle was counterbalanced and placed in each cage. Measurements were taken after 24 h. Preference ratios were calculated as (0.15% saccharin consumed)/(water consumed + 0.15% saccharin consumed).

Anxiety testing

Single-housed mice were put into the behaviour room to habituate 1 hour before the experiment and were injected with vehicle or danuglipron (30 mg kg^{-1}) at ZT11.5 or orforglipron (1 mg kg^{-1}) at ZT8.5. Experiments were performed from ZT12.5 to ZT13.5. Mice were placed individually in the centre of the arena (50.8 cm diameter with 24 cm walls) with dim light (around 25 lux) and allowed to explore freely for 5 min. In the open field test, the arena is a circular box with a diameter of 50 cm. In the elevated plus maze test, the arena is an elevated cross (height of 40 cm), with two closed arms (5 × 30 cm), and two open arms of the same dimension. Mouse movement was captured by a camera, and nose points and centre points were tracked by Ethovision software. The arena was cleaned with 70% ethanol between trials. In the open field test, the total centre area (33.9 cm diameter) was defined as the centre zone. Total distance travelled and percentage of time in the centre zone were measured. In the elevated plus maze, head dip zone was defined as within 5 cm outside of the open arm. Total distance travelled, time spent in each arm and head dip activity were measured in Ethovision.

Home-cage monitoring of *Glp1r*^{S33W} mice

Mice were single-housed and acclimatized to PhenoTyper home cages (Noldus) for 5 days before testing. Each cage was placed inside a light-tight behavioural box equipped with programmable lighting, allowing precise control over light exposure. Cages were maintained on a 12:12-h LD cycle. During acclimatization, mice had ad libitum access

to standard chow (SD) in a food hopper, and to water bottles, running wheels, shelters and bedding. Mice that failed to meet a baseline criterion of at least 50 food-hopper head entries between ZT12 and ZT14 were excluded to ensure sufficient engagement with the feeding set-up. Of 59 mice tested, 12 did not meet this threshold and were excluded.

To capture the peak behavioural effects of each drug, injections were timed on the basis of their pharmacokinetics and previous results (Fig. 1), and all behavioural assays were done at the same ZT, with paired controls accounting for differences in injection timing. For testing, lithium chloride (125 mg kg^{-1}) or vehicle was administered 5 min before recording. Danuglipron (30 mg kg^{-1}) or vehicle was administered at ZT11.5, liraglutide (0.3 mg kg^{-1}) or vehicle at ZT10 and orforglipron (1 mg kg^{-1}) or vehicle at ZT8. Injections were counterbalanced across mice. Behaviour was recorded for 2 hours starting at ZT12. In the fed condition, mice had access to a HFD placed on the cage floor from ZT11 to ZT12. At ZT12, the HFD was removed and only SD remained in the food hopper. Fed mice were habituated to HFD exposure (1 hour per day) for 3 days before cage habituation. All mice were also habituated to handling and saline injections for 3 days before recording.

PhenoTyper sensors continuously recorded food-hopper entries, water licks and wheel rotations. Behavioural sessions were video-recorded from above using infrared cameras (960 × 540 pixels, 25 fps, greyscale). Videos were cropped to 2-hour segments using Adobe Premiere Pro and re-encoded using H.264 compression with FFmpeg for consistent playback and frame indexing.

Machine-learning-assisted behaviour classification. Mouse pose tracking was performed using SLEAP (v.1.3.3)[24,25]. Nine keypoints were tracked: nose, ears (left and right), tail base and five body centre points (Supplementary Fig. 1b). A total of 11,847 frames were manually labelled across 19 representative videos. These were split into training (9,693 frames; 80%), validation (1,077 frames; 10%) and test (1,077 frames; 10%). The test set was drawn from a separate video to ensure independence and to capture a variety of poses and behaviours. The model was trained using a U-Net architecture with max stride 32, 16 filters and ±180° rotation, using default parameters for the single-mouse pipeline. On the held-out test set, the model achieved a mean Object-Keypoint Similarity (OKS) of 0.92, an OKS-based Visual Object Classes (VOC) mean average precision of 0.84, and an OKS-based VOC mean average recall of 0.89.

Representative heat maps of the nose keypoint were generated to visualize the spatial occupancy patterns across the home-cage PhenoTyper. These heat maps were created by cropping to exclude cage walls and binning into 62 × 27 spatial grids.

Although only the nose keypoint was used for heat-map visualization, Keypoint-MoSeq[24,25] was applied to the full set of nine tracked keypoints to infer behavioural syllables from 80 h of keypoint data. After alignment and centring, four latent dimensions explained 90% of variance. To determine the appropriate timescale for behavioural segmentation, we ran an automatic κ scan in Keypoint-MoSeq and identified values that yielded syllable durations that were consistent with previous mouse studies[25]. We then fitted models using the three closest κ values and selected the one that produced syllables most consistent with recognizable behavioural motifs. This final model used a κ value of 10^5 and identified 91 syllables. Syllables that comprised at least 0.5% of frames were included. Those between 0.01% and 0.5% were retained; syllables less than 0.01% were excluded. Syllables were grouped into behavioural categories (Supplementary Fig. 3) by two trained raters. Some syllables captured blended actions (for example, groom/sniff), probably owing to overhead view limitations. Low-quality and background syllables (around 1%) were excluded.

Syllable analysis. Before manual curation, syllable data generated by MoSeq were analysed to assess behavioural differences across treatment groups. For each drug condition (LiCl, danuglipron, liraglutide and orforglipron), syllable use was compared with those of their respective paired control groups. In addition, syllable transition patterns were examined by comparing bigram-normalized transition probabilities between drug-treated and control mice.

All analyses were performed using code based on previous MoSeq analyses[25,53]. Owing to the large number of syllables detected, only statistically significant ($P < 0.05$) or frequently occurring syllables were visualized in most figures. However, all syllables were included in the full analysis.

Behaviour localization and categorization. The locations of the food hopper, water spout and shelter were identified using OpenCV (2024), and corresponding regions of interest were defined. The nose keypoint was used to detect entries into the food and water regions of interest; centre point 3 was used for shelter entry. Behaviours were labelled contextually (for example, 'sniff by food' versus 'sniff' elsewhere). This produced 22 distinct behaviours, grouped into 5 broader categories on the basis of behavioural similarity and transition frequency: rest or groom in shelter; groom; move or explore; food-motivated; and drink. In some analyses (Extended Data Figs. 5c and 6k,q,w), movement within the shelter was analysed separately. 'Pause' outside the shelter was excluded owing to lack of behavioural relevance. These behaviours captured 95.7% of all behavioural time across videos. For each 2-hour recording, time spent per behavioural category was normalized to total behavioural time.

Grouped behaviour analysis. Behavioural proportions were analysed using beta-distributed generalized linear mixed-effects models, with mouse as a random effect. Different link functions (for example, logit or cloglog) were used depending on the distribution of each behaviour. Proportions in the control condition were normalized to mean = 1; treatment data for each mouse were scaled using this normalization to highlight the magnitude of change. For network analysis, transition probabilities between behaviours were computed for each mouse and normalized by the total outgoing transitions from the starting behaviour. Probabilities were then combined across both directions (A↔B) to generate undirected transition measures and averaged per group. Behavioural transition networks were generated using NetworkX[54], with line colour scaled by the global maximum-normalized transition probability across all plotted groups. Node size reflects average bout length and was normalized to the global maximum across all groups, then manually scaled in Illustrator (for example, a value of 0.86 corresponds to 86% of the maximum node size). PCA was conducted on selected standardized behavioural feature data to reduce dimensionality. The main analysis code is available on GitHub (see 'Code availability').

Electrophysiology recordings

Brain slice preparation. At least a month before recordings, AAV-DIO-mGlp1r or AAV-DIO-hGLP1R was co-injected 1:1 with AAV-DIO-eYFP into *Glp1r-Cre* mice so that YFP marked Cre-positive neurons competent to express the receptor. Preparation of acute brain slices for patch-clamp electrophysiology experiments was modified from standard protocols previously described[55–57]. Mice were anaesthetized with isoflurane and decapitated. The brains were rapidly removed and kept in modified chilled artificial cerebrospinal fluid (ACSF) (1 °C) containing 93 mM *N*-methyl-D-glucamine, 2.5 mM KCl, 1.25 mM NaH_2PO_4, 20 mM HEPES, 5 mM L-ascorbic acid (sodium salt), 2 mM thiourea, 3 mM sodium pyruvate, 0.5 mM $CaCl_2$, 10 mM $MgSO_4$, 25 mM D-glucose, 12 mM *N*-acetyl-L-cysteine and 30 mM $NaHCO_3$, with pH adjusted to 7.2–7.4 using HCl (osmolarity 310 mOsm). Slices were continuously oxygenated with 95% O_2 and 5% CO_2 throughout the preparation. Coronal brain sections (300 µm) were prepared using a Leica Microsystems VT1200 vibratome. Slices were collected and placed in ACSF containing 125 mM NaCl, 2.5 mM KCl, 1.25 mM NaH_2PO_4, 2 mM $CaCl_2$, 1 mM $MgCl_2$, 0.5 mM L-ascorbic acid, 10 mM glucose, 25 mM $NaHCO_3$

and 2 mM Na-pyruvate (osmolarity 310 mOsm), warmed to 37 °C for 30 min and then kept at room temperature for up to 5 hours.

Recordings. Brain slices were placed in a chamber superfused (around 3 ml per min) with continuously oxygenated ACSF solution warmed to 32 ± 1 °C. Human-GLP1R- or mouse-GLP1R-expressing amygdala neurons were identified by video microscopy on the basis of the expression of eYFP and regional markers. Whole-cell electrophysiology recordings were performed using a Multiclamp 700B amplifier with signals digitized by a Digidata 1550B digitizer. Currents were amplified, low-pass-filtered at 2 kHz and sampled at 35 kHz. Borosilicate electrodes were fabricated using a Brown–Flaming puller (model P1000, Sutter Instruments) to have pipette resistances between 2.5 mΩ and 4.5 mΩ. Current-clamp recordings of membrane potentials were collected in an ACSF solution identical to that used for preparation of brain slices. The internal solution contained the following: 120 mM K-gluconate, 10 mM NaCl, 2 mM $MgCl_2$, 0.5 mM K_2EGTA, 10 mM HEPES, 4 mM Na_2ATP and mM 0.3 NaGTP, pH 7.2 (osmolarity 290 mOsm). Resting membrane potential was recorded as previously described[55,56]. After 5 min of baseline membrane potential recordings, 30 µM of danuglipron was perfused for 5 min. Action potentials were generated using a current injection ramp (100 pA s^{-1}) before and after 5 min of danuglipron perfusion to determine effects on time to action potential threshold. Danuglipron powder (Selleck, S9851) was dissolved to 30 mg ml^{-1} in 100% ethanol with gentle sonication, then diluted to 3 mg ml^{-1} (5.4 mM) in vehicle (1 M NaOH, 2% Tween 80, 5% PEG 400, 5% dextrose). For electrophysiology recordings, 280 µl of this stock was added to 50 ml ACSF (1:180 dilution) to yield a final danuglipron concentration of 30 µM, corresponding to final concentrations of approximately 0.056% ethanol, 0.011% Tween 80 and 0.028% PEG 400.

Statistics. Electrophysiology recordings were analysed using ClampFit (v.11.2). All statistical comparisons were made using the appropriate test in GraphPad Prism (v.10.4.0). Membrane potential and action potential properties underwent descriptive statistics followed by normality and lognormality tests using a Gaussian distribution. Data were assessed for normality using the D'Agostino–Pearson omnibus normality test, Anderson–Darling test, Shapiro–Wilk test and Kolmogorov–Smirnov test with Dallal–Wilkinson–Lilliefors for *P* values. Cells with unstable resting membrane potentials were excluded from the analysis and no cells were considered statistical outliers. Initial testing was followed by Tukey's test for drug effect comparison. Data are presented as individual data points and/or mean ± s.e.m.

Fibre photometry recordings

Calcium recordings (GCaMP). Mice underwent 20-min daily habituation sessions over 2 consecutive days to acclimatize to the fibre-optic cable (Doric Lenses, Ø 400-µm core, 0.57 numerical aperture). On the test day, mice were injected with vehicle, danuglipron (30 mg kg^{-1}) or liraglutide (0.3 mg kg^{-1}) 2 hours before recording. The order of injections was randomized to avoid order effects. After the 2-hour post-injection period, mice were connected to patch cables that were interfaced with rotary joints to enable free movement. Recordings were done for 1 hour in the mouse home cage without food and water. Fibre photometry data were recorded using fluorescent signals from both calcium-dependent (465 nm) and calcium-independent isosbestic (405 nm) excitation wavelengths (Doric). The isosbestic (405 nm) signal served to control for artefacts. The light power of the fibre-optic cable was measured before each experiment and maintained at approximately 20–30 µW for both the calcium-independent isosbestic (405 nm) and the calcium-dependent (465 nm) signal.

Calcium analysis (GCaMP). The isosbestic signal (405 nm) was fitted to the calcium-dependent (465 nm) signal using a linear least squares method implemented in a custom MATLAB script, and $\Delta F/F$ was calculated as (465 nm − fitted 405 nm)/fitted 405 nm. For *z*-score calculation, we then implemented a paired *z*-score normalization: for each mouse, we used the full $\Delta F/F$ time series from its vehicle session to calculate $\mu_{(\text{vehicle})}$ (mean) and $\sigma_{(\text{vehicle})}$ (s.d.), and all $\Delta F/F$ values—both vehicle and drug—were converted to *z*-scores via $[\Delta F/F(t) - \mu_{(\text{vehicle})}]/\sigma_{(\text{vehicle})}$, anchoring comparisons to a common baseline distribution. Significant calcium transients were detected on these *z*-scored traces using a threshold of median + 2 s.d. (of the entire recording) with a minimum duration of 1.5 s; events were counted per trial and displayed as heat maps of *z*-score to ensure full transparency of raw recording structure. Finally, the AUC of each mouse's complete *z*-scored trace was calculated using a custom MATLAB script to validate overall activity differences between conditions. Heat maps were generated in MATLAB using min–max normalization, scaled to a range of 0–1. For each mouse, the normalization range was determined on the basis of the vehicle condition: the average of the lowest 360 data points was set as the minimum, and the average of the highest 360 data points was set as the maximum. This normalization range, derived from the vehicle condition, was then applied to the corresponding paired danuglipron or liraglutide data for the same mouse. A moving average with a window and bin size of 10 smoothed the data, which were then plotted as a heat map. Mice with missed virus injection or off-target fibre placement were excluded from analysis.

Dopamine recordings (dLight). Mice (WT, *Glp1r-Cre* or $Glp1r^{S33W}$) were single-housed and habituated to the fibre-optic cable and HFD for 1 hour over 2 consecutive days. On the test day, mice received an injection of either a drug (liraglutide (0.3 mg kg^{-1}), danuglipron (30 mg kg^{-1}) or orforglipron (1 mg kg^{-1})) or vehicle on different days, with the order of drug versus vehicle injections randomized. Liraglutide and danuglipron were administered 2 hours before recording, whereas orforglipron was given 4 hours earlier. Fibre photometry data were recorded as described above. Fluorescent signals were collected from both dopamine-dependent (465 nm) and dopamine-independent isosbestic (405 nm) excitation wavelengths. During the testing sessions, small pellets of HFD (around 10 mg) were dropped into a cup at 2-minute intervals after the mice retrieved the pellet. Five to six trials were done per mouse. The recording session was video-recorded to time-stamp food retrieval time, and recordings were done during the light phase, between ZT3 and ZT6.

Dopamine analysis (dLight). The isosbestic signal (405 nm) was fitted to the dopamine-dependent (465 nm) signal using a linear least squares method implemented in a custom MATLAB script. Then $\Delta F/F$ was calculated as (465 nm − fitted 405 nm)/fitted 405 nm. To account for inter-mouse differences in signal intensities, *z*-scores were calculated for the $\Delta F/F$ signals. The baseline period for each food trial was defined as the 30-s interval before food retrieval. The mean and standard deviation of the baseline period were used to compute the *z*-scores, with the formula: $z\text{-score} = (F - F\mu_{(\text{baseline})})/\text{s.d.}_{(\text{baseline})}$, where *F* is the 405 nm corrected 465 nm signal ($\Delta F/F$), $\mu_{(\text{baseline})}$ is the mean and $\text{s.d.}_{(\text{baseline})}$ is the standard deviation of the baseline period. Video frames were analysed to determine the exact time stamp when the mouse retrieved the pellet, which was defined as time 0 for each retrieval. The 30-s window centred around the food retrieval time was extracted. The AUC and maximum fluorescence *z*-scored within the food retrieval window were further extracted and analysed for quantification of dopaminergic activity. Five food trials were averaged per mouse. Mice with missed virus injections or off-target fibre placements were excluded from the analysis.

Data and statistical analyses

Sample sizes were determined on the basis of our previous experiments and experience with these assays, with the goal of providing adequate power to detect biologically meaningful effects. No formal

a priori statistical power calculations were performed. Investigators were not blinded to group allocation during data collection and analysis, except where explicitly indicated. All data are presented as mean ± s.e.m. unless otherwise noted. Statistical tests including paired or unpaired two-tailed *t*-tests, Kruskal–Wallis tests, Wilcoxon signed-rank tests, one-way ANOVA, two-way or repeated-measures ANOVA (with Bonferroni correction or Tukey's HSD post-hoc tests) and linear mixed-effects models with beta regression (with Holm post-hoc test) were performed using RStudio (v.4.1.2, v.4.3.0), Python (v.3.11.5), JupyterLab (v.3.6.3), MATLAB (R2024b), GraphPad Prism (v.10.4.0) or Microsoft Excel (2024). Brief descriptions of all experiments in each figure panel, sample sizes, mean ± s.e.m, statistical tests, test statistics and *P* values are presented in Supplementary Table 1. $^{*}P < 0.05$, $^{**}P < 0.01$ and $^{***}P < 0.001$.

Reporting summary

Further information on research design is available in the Nature Portfolio Reporting Summary linked to this article.

Data availability

All data are available on LabArchives at https://mynotebook.labarchives.com/share/Guler%2520Lab%2520Notebook/MTQuM3wxMTY0NDYxLzExL1RyZWVOb2RlLzI1NDM4MDU2N3wzNi4z. Source data are provided with this paper.

Code availability

All code is available on GitHub at https://github.com/UVACircMetNeuLab/glp1r-reward-circuit.

52. Szelenyi, E. R. et al. An arginine-rich nuclear localization signal (ArgiNLS) strategy for streamlined image segmentation of single cells. *Proc. Natl Acad. Sci. USA* **121**, e2320250121 (2024).
53. Wiltschko, A. B. et al. Revealing the structure of pharmacobehavioral space through motion sequencing. *Nat. Neurosci.* **23**, 1433–1443 (2020).
54. Hagberg, A., Swart, P. J. & Schult, D. A. Exploring network structure, dynamics, and function using NetworkX. In *Proc. 7th Python in Science Conference* (*SciPy*) (eds Varoquaux, G. et al.) 11–15 (SciPy, 2008).
55. Ottolini, M., Barker, B. S., Gaykema, R. P., Meisler, M. H. & Patel, M. K. Aberrant sodium channel currents and hyperexcitability of medial entorhinal cortex neurons in a mouse model of SCN8A encephalopathy. *J. Neurosci.* **37**, 7643–7655 (2017).
56. Wengert, E. R. et al. Somatostatin-positive interneurons contribute to seizures in SCN8A epileptic encephalopathy. *J. Neurosci.* **41**, 9257–9273 (2021).
57. Bunton-Stasyshyn, R. K. A. et al. Prominent role of forebrain excitatory neurons in SCN8A encephalopathy. *Brain* **142**, 362–375 (2019).

Acknowledgements We thank the members of the A.D.G., C.D.D., J.N.C. and I. Provencio laboratories (University of Virginia) and A. Hardaway (University of Alabama at Birmingham) for comments and suggestions on the preparation of the manuscript; S. A. Mancuso for technical help; A. Pathak, T. Pereira and C. Weinreb for technical advice; A. Spano for developing the three viral constructs; S. He and R. Klein for sharing their processed single-cell RNA-seq CeA dataset; M. Yorek for verifying viral targeting in CeA-electrophysiology mice; and the Genetically Engineered Murine Model (GEMM) Core (University of Virginia) for helping with the CRISPR–Cas9 development of our mouse model. MERFISH datasets were obtained from the Allen Brain Atlas, provided by the Allen Institute for Brain Science. We used large language models (OpenAI, Anthropic) as an aid for drafting and grammar proofing the manuscript. This work was supported by NIH R35GM140854 (A.D.G.); NIH R01NS111220 (C.D.D.); NIH R01HL153916 and American Diabetes Association Pathway to Stop Diabetes Award 1-18-INI-14 (J.N.C.); NIH R01 NS122834 and NIH R01 NS120702 (M.K.P.); University of Virginia Brain Institute Seed Funding 2023 and 2024 (A.D.G. and C.D.D.) and 2024 and 2025 (A.D.G. and J.N.C.); University of Virginia Brain Institute Presidential Fellowship in Collaborative Neuroscience (E.N.G.); University of Virginia National Science Foundation, EXPAND Traineeship NSF NRT-ROL 2021791 (E.N.G. and I.R.S.); University of Virginia Interdisciplinary Fellowship in Quantitative Neurobiology of Behavior (T.B.G.); and the GEMM core, which is partially supported by the funding of NIH-NCI CCSG P30 CA044579.

Author contributions Conceptualization: E.N.G., T.B.G., I.R.S., A.B.K., J.N.C., C.D.D. and A.D.G. Data curation: E.N.G., T.B.G., I.R.S., T.C.J.D., S.O., Y.Z., O.L., G.T. and O.K. Formal analysis: E.N.G., T.B.G., I.R.S., T.C.J.D. and A.D.G. Funding acquisition: E.N.G., T.B.G., I.R.S., M.K.P., J.N.C., C.D.D. and A.D.G. Investigation: E.N.G., T.B.G., I.R.S., A.K.B., O.L., Y.Z., Y.S., T.C.J.D., G.T., O.K., E.J.S., M.C., N.J.C., A.N.W., O.Y.C., S.O., W.L., A.A., K.M., K.I.W., S.M.-L., A.K., G.v.G., C.X.G., G.M. and O.A.D. Methodology: E.N.G., T.B.G., I.R.S., A.B.K. and A.K.B. Project administration: A.D.G. Resources: K.T.B., L.S.Z., M.K.P., J.N.C., C.D.D. and A.D.G. Supervision: E.N.G., T.B.G., I.R.S., K.T.B., L.S.Z., M.K.P., J.N.C., C.D.D. and A.D.G. Validation: E.N.G., T.B.G., I.R.S., A.K.B., C.D.D. and A.D.G. Visualization: E.N.G., T.B.G. and I.R.S. Writing (original draft): E.N.G., T.B.G., I.R.S., C.D.D. and A.D.G. Writing (review and editing): E.N.G., T.B.G., I.R.S., J.N.C., C.D.D. and A.D.G.

Competing interests The authors declare no competing interests.

Additional information

Supplementary information The online version contains supplementary material available at https://doi.org/10.1038/s41586-026-10444-4.

Correspondence and requests for materials should be addressed to Christopher D. Deppmann or Ali D. Güler.

Peer review information *Nature* thanks the anonymous reviewers for their contribution to the peer review of this work. Peer reviewer reports are available.

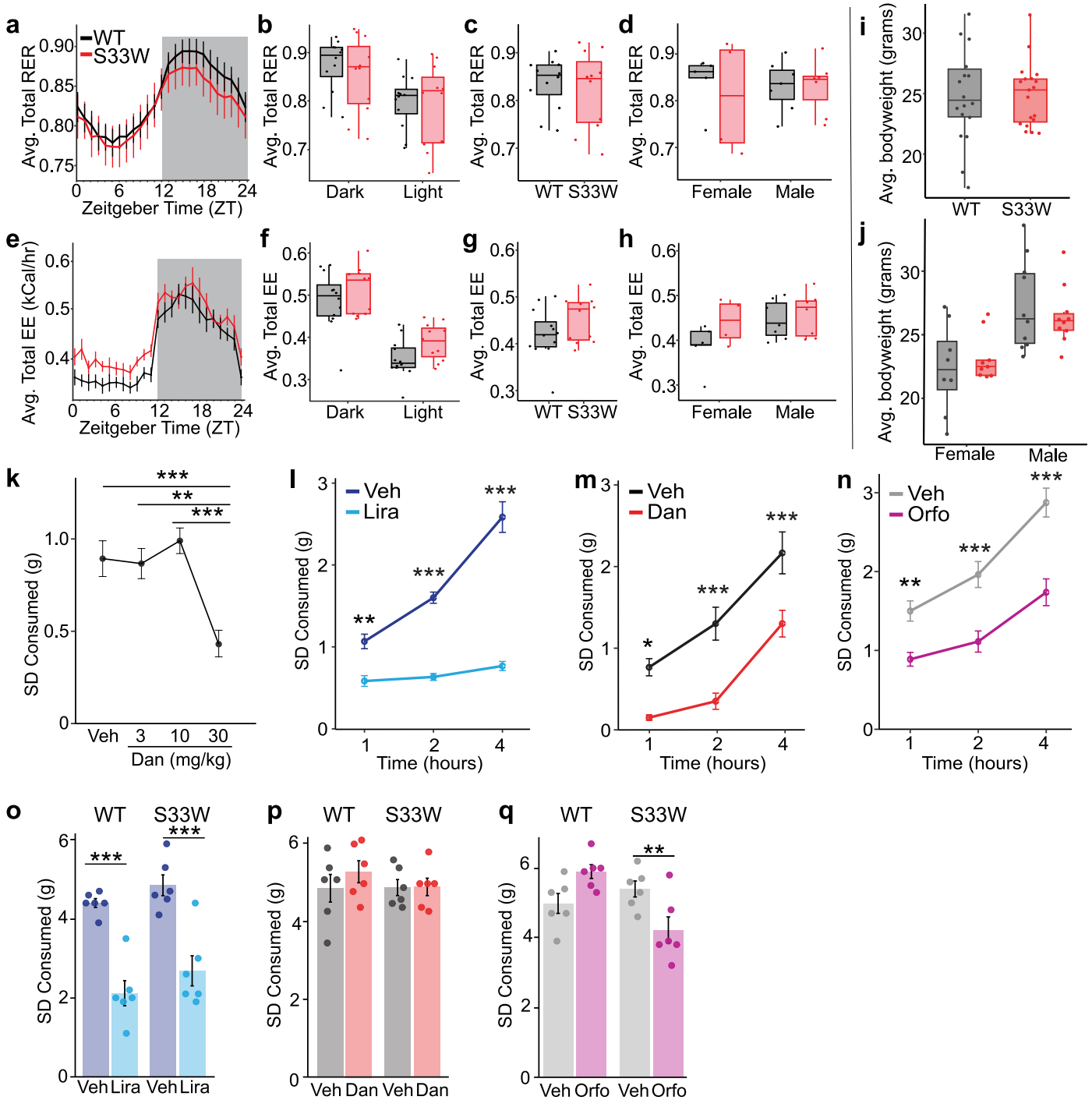

Extended Data Fig. 1 | Metabolic profiling of WT and *Glp1r*^{S33W} mice and effects of GLP1RAs on SD intake. a,**e**, Diurnal rhythms averaged over 3 days of RER (**a**) and energy expenditure (EE; **e**) in WT ($n = 12$) and S33W ($n = 11$) mice. **b**,**c**,**f**,**g**, Dark/light phase and total 24-hour RER (**b**,**c**) and EE (**f**,**g**). **d**,**h**, Total 24-hour RER (**d**) and EE (**h**) by sex (WT males $n = 7$, females $n = 5$; S33W males $n = 7$, females $n = 4$). **i**,**j**, Baseline body weight (10-20 weeks). **i**, WT ($n = 18$) and S33W ($n = 19$). **j**, Baseline body weight by sex (WT females $n = 8$, WT males $n = 10$; *Glp1r*^{S33W} females $n = 9$; S33W males $n = 10$). **k**, Two-hour SD intake (ZT12-14) following vehicle or danuglipron (3, 10, 30 mg/kg) (3 mg/kg, $n = 9$; 10 mg/kg, $n = 8$; 30 mg/kg, $n = 15$). **l**–**n**, Post-fast refeeding (1, 2, 4 h) after liraglutide (**l**, n = 6), danuglipron (**m**, $n = 6$), or orforglipron (**n**, $n = 8$) versus vehicle in *Glp1r*^{S33W} mice. **o**–**q**, 24-hour SD intake after liraglutide (**o**), danuglipron (**p**), or orforglipron (**q**) in WT and *Glp1r*^{S33W} mice ($n = 6$/injection). Two-way ANOVA with Bonferroni correction was used on panels: **b**, **d**, **f**, **h**, **j**, **l**–**q**; Welch's t-test was applied in **c**, **g**, and **i**; one-way ANOVA with Tukey's HSD was used for **k**. Data are median ± Q1–Q3 for metabolic and body weight panels and mean ± s.e.m. for intake studies. For all box plots, boxes represent the interquartile range (Q1–Q3) with the median indicated; whiskers extend to 1.5 × IQR. All data points are displayed, including the minimum and maximum values. *$P < 0.05$; **$P < 0.01$; **$P < 0.001$.

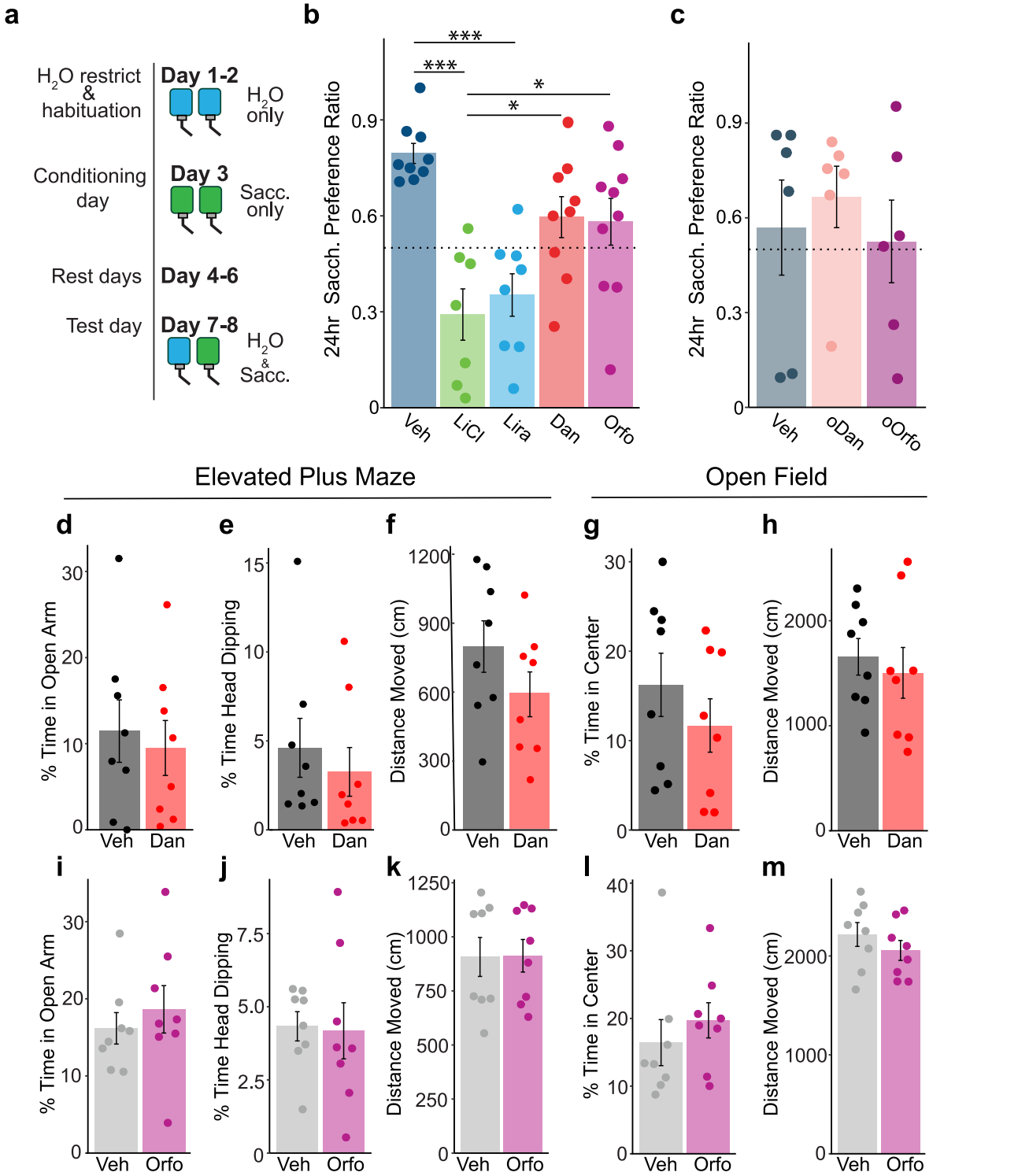

Extended Data Fig. 2 | Effects of GLP1RAs on CTA and anxiety measures. **a**, Pipeline for CTA protocol. **b**, 24-hour saccharin preference after injections of vehicle (Veh), lithium chloride (LiCl), liraglutide (Lira), danuglipron (Dan), or orforglipron (Orfo) (Veh $n = 9$, LiCl $n = 7$, Lira $n = 8$, Dan $n = 9$, Orfo $n = 10$; one-way ANOVA with Tukey's HSD correction, $^{*}P < 0.05$, $^{***}P < 0.001$). **c**, 24-hour saccharin preference after oral administration of oral Veh (oVeh), oral Dan (oDan), or oral Orfo (oOrfo) ($n = 6$ per injection, one-way ANOVA with Tukey's HSD correction). **d**–**m**, EPM and OFT anxiety tests after injections of (**d**–**h**) vehicle (Veh) or danuglipron (Dan) and (**i**–**m**) vehicle (Veh) or orforglipron (Orfo). *Glp1r*^{S33W} mice were injected with Veh/Dan at ZT11.5 or Veh/Orfo at ZT8.5 and tested at ZT12.5. For the EPM test, the percentage of time spent in open arms, percentage of time spent head dipping, and distance travelled were measured. For the OFT, the percentage of time spent in the centre (defined as 4/9 of centre area) and distance travelled were measured ($n = 8$ per injection, Welch's t-test). Data are mean ± s.e.m. $^{*}P < 0.05$; $^{**}P < 0.01$; $^{***}P < 0.001$.

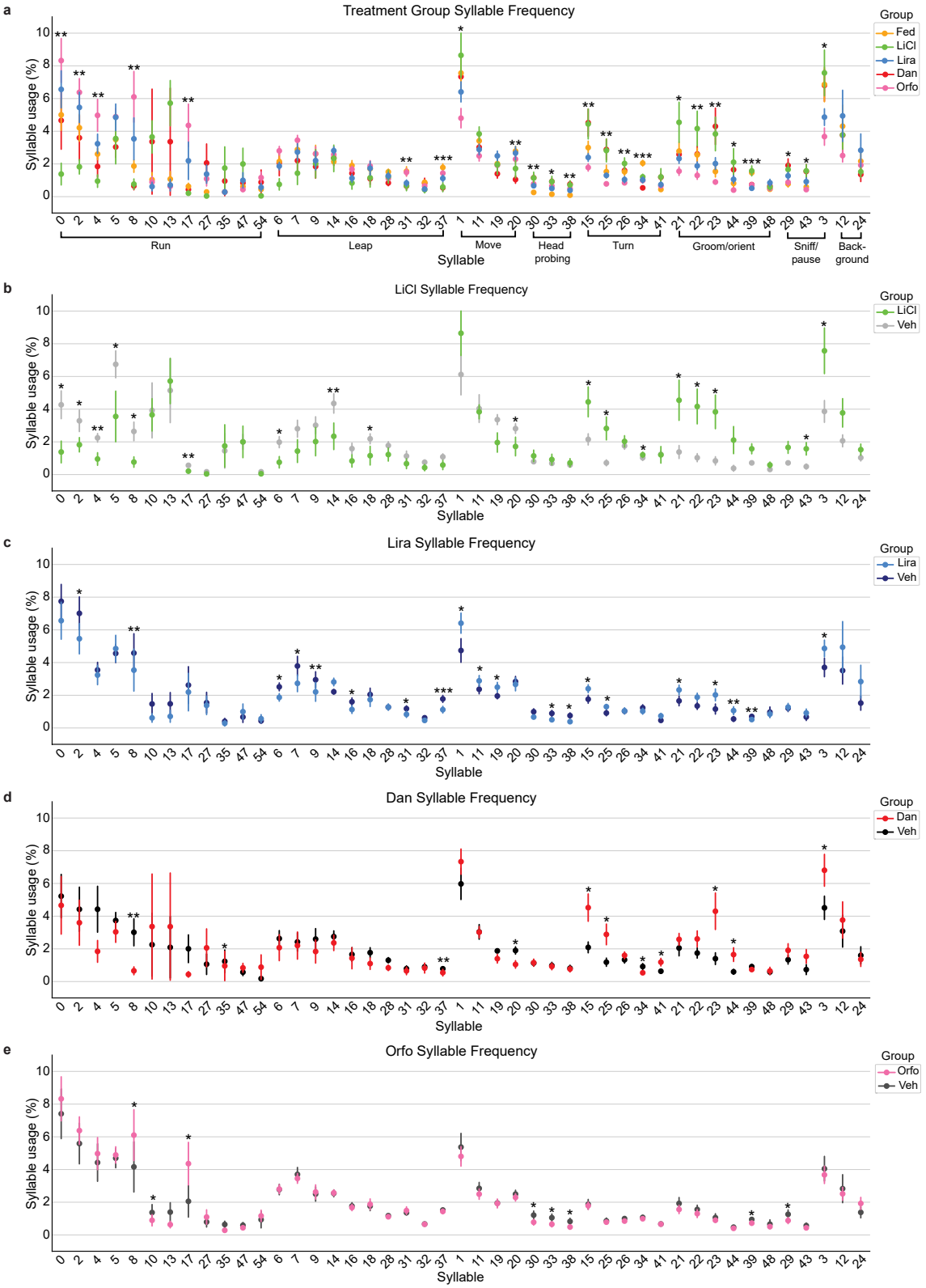

Extended Data Fig. 3 | Behavioural syllable frequency across drug groups. **a**–**e**, Percentage of behavioural syllable usage occurring with a probability > 0.05 in the full dataset. **a**, Percentage of syllables across all drug groups and the fed condition. Group differences were assessed using one-way ANOVA ($n = 10$ Fed, $n = 6$ LiCl, $n = 9$ Lira, $n = 9$ Dan, $n = 10$ Orfo; $^{*}P < 0.05$; $^{**}P < 0.01$; $^{***}P < 0.001$). **b**, Syllable percentage comparison between LiCl and its paired control (Veh), assessed by paired *t*-test ($n = 6$ LiCl, $n = 6$ Veh; $^{*}P < 0.05$, $^{**}P < 0.01$). **c**, Syllable percentage comparison between Lira and its paired control ($n = 9$ Lira, $n = 9$ Veh; $^{*}P < 0.05$; $^{**}P < 0.01$; $^{***}P < 0.001$). **d**, Syllable percentage comparison between Dan and its paired control ($n = 9$ Dan, $n = 9$ Veh; $^{*}P < 0.05$, $^{**}P < 0.01$). **e**, Syllable percentage comparison between Orfo and its paired control ($n = 10$ Orfo, $n = 10$ Veh; $^{*}P < 0.05$). All data are mean ± s.e.m.

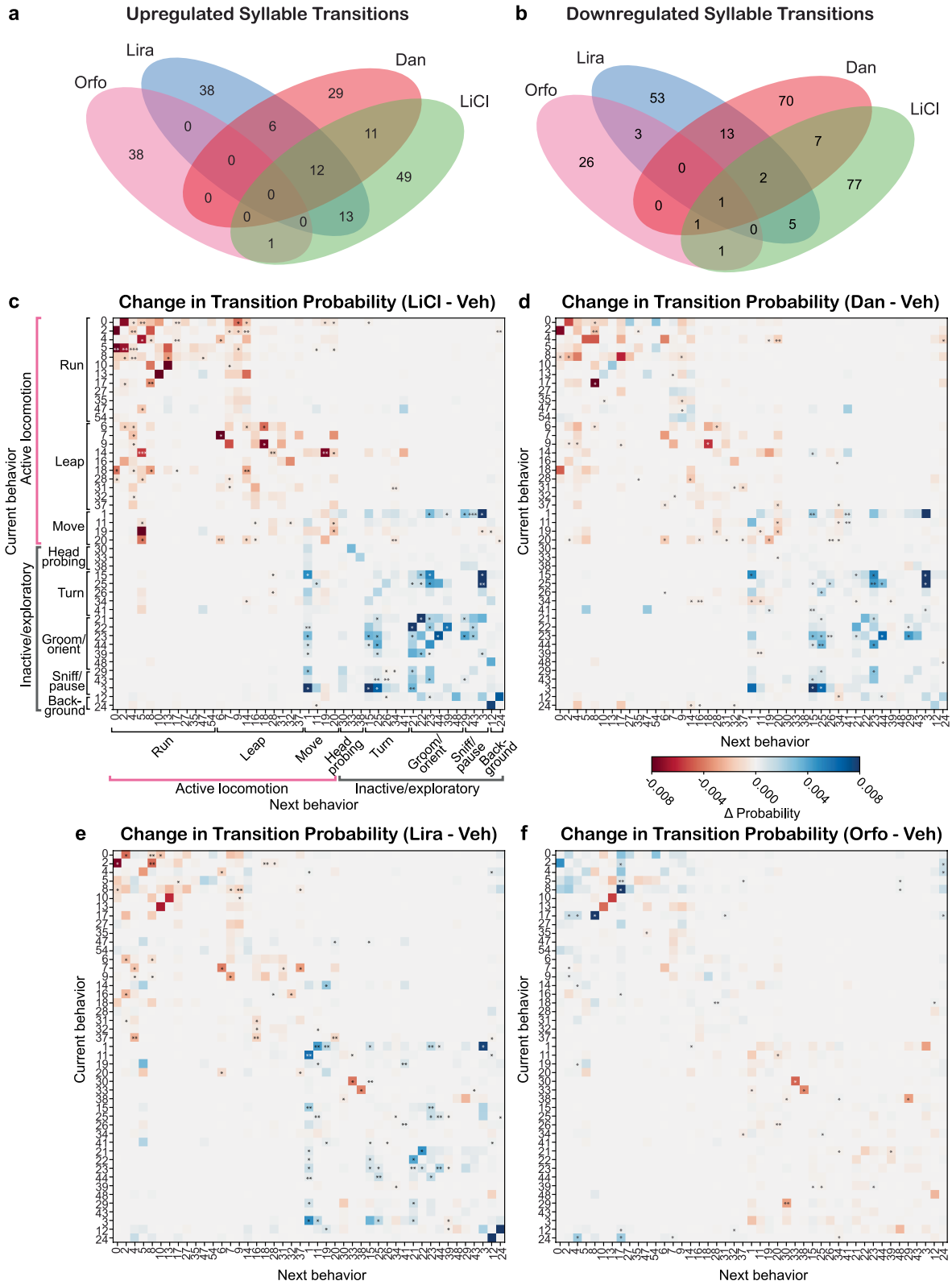

Extended Data Fig. 4 | Behavioural syllable transitions across drug conditions. a,**b**, Number of statistically significant normalized bigram transitions ($P < 0.05$) for each drug condition (Orfo/Veh, Lira/Veh, Dan/Veh, LiCl/Veh), assessed using paired *t*-tests ($n = 10$ Orfo, $n = 9$ Lira, $n = 9$ Dan, $n = 6$ LiCl). Venn diagrams illustrate the overlap of significant transitions across paired group comparisons. **a**, Upregulated transitions under drug conditions. **b**, Downregulated transitions. **c**–**f**, Transition heat maps showing changes from vehicle control for each drug condition. Red indicates decreased transitions on drug; blue indicates increased transitions. **c**, LiCl; **d**, danuglipron; **e**, liraglutide; **f**, orforglipron. Syllables are grouped by broad behavioural categories. Some asterisks indicating significance are coloured white for visibility (*$P < 0.05$; **$P < 0.01$; ***$P < 0.001$).

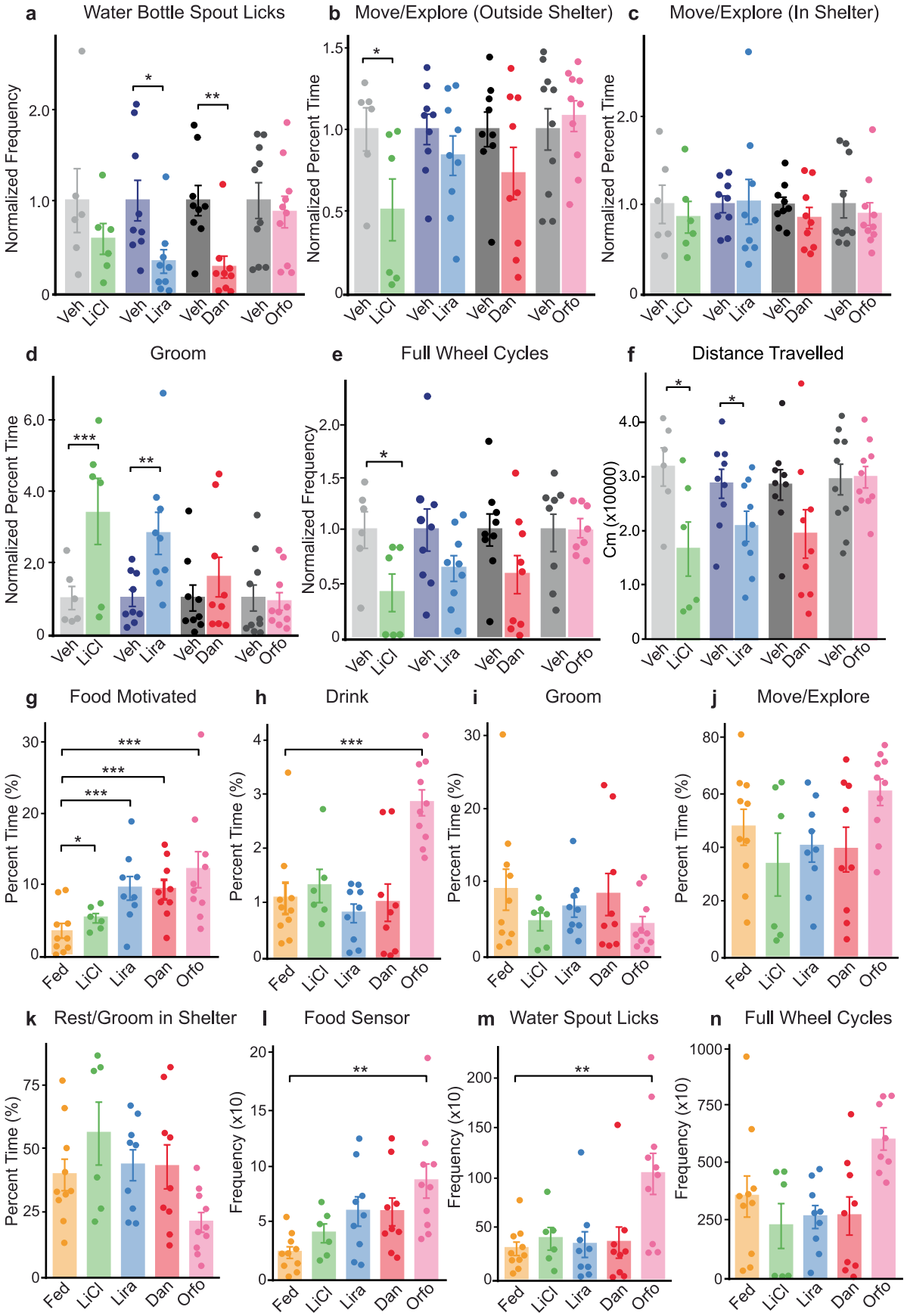

Extended Data Fig. 5 | See next page for caption.

Extended Data Fig. 5 | Percentage of time engaged in behaviours, sensor activity and distance travelled. a, Sensor data normalized to paired controls: Total number of water spout licks (frequency). (paired *t*-test on raw frequency data). **b**–**d**, Percentage of time spent performing each behaviour, normalized to paired control groups for liraglutide-, danuglipron-, orforglipron-, and LiCl-treated mice. (n = 6 Veh/LiCl, n = 9 Veh/Lira, n = 9 Veh/Dan, n = 10 Veh/Orfo, generalized linear mixed-effects model (GLMM) with beta regression on raw (non-normalized) proportion data, comparing treatment to control with random intercept for mouse ID (paired)). **e**, Sensor data normalized to paired controls: Total number of complete wheel rotations. (paired *t*-test on raw frequency data; n = 6 Veh/LiCl, n = 9 Veh/Lira, n = 9 Veh/Dan, n = 8 Veh/Orfo). **f**, Total distance travelled (centimetres) tracked using the neck/upper back keypoint of mice administered LiCl, danuglipron (Dan), liraglutide (Lira), orforglipron (Orfo), or their paired controls (Veh). (Paired t-test, n = 6 Veh/LiCl, n = 9 Veh/Dan, n = 9 Veh/Lira, n = 10 Veh/Orfo). **g**–**k**, Percentage of time spent performing behaviours across unpaired treatment groups. (n = 10 fed, n = 6 LiCl, n = 9 Lira, n = 9 Dan, n = 10 Orfo, GLMM with beta regression on raw proportion data, comparing fed group to each treatment group with Holm-corrected post-hoc tests). **l**–**n**, Sensor-based activity (one-way ANOVA with post-hoc comparisons of each group vs fed, Holm correction applied): **l**, Total number of head entries at the food hopper (TTL beam breaks) (n = 10 fed, n = 6 LiCl, n = 9 Lira, n = 9 Dan, n = 10 Orfo); **m**, Total number of licks from the water spout (n = 10 fed, n = 6 LiCl, n = 9 Lira, n = 9 Dan, n = 10 Orfo); **n**, Total number of complete wheel turns (n = 10 fed, n = 6 LiCl, n = 9 Lira, n = 9 Dan, n = 8 Orfo). All data are mean ± s.e.m. *P < 0.05; **P < 0.01; ***P < 0.001.

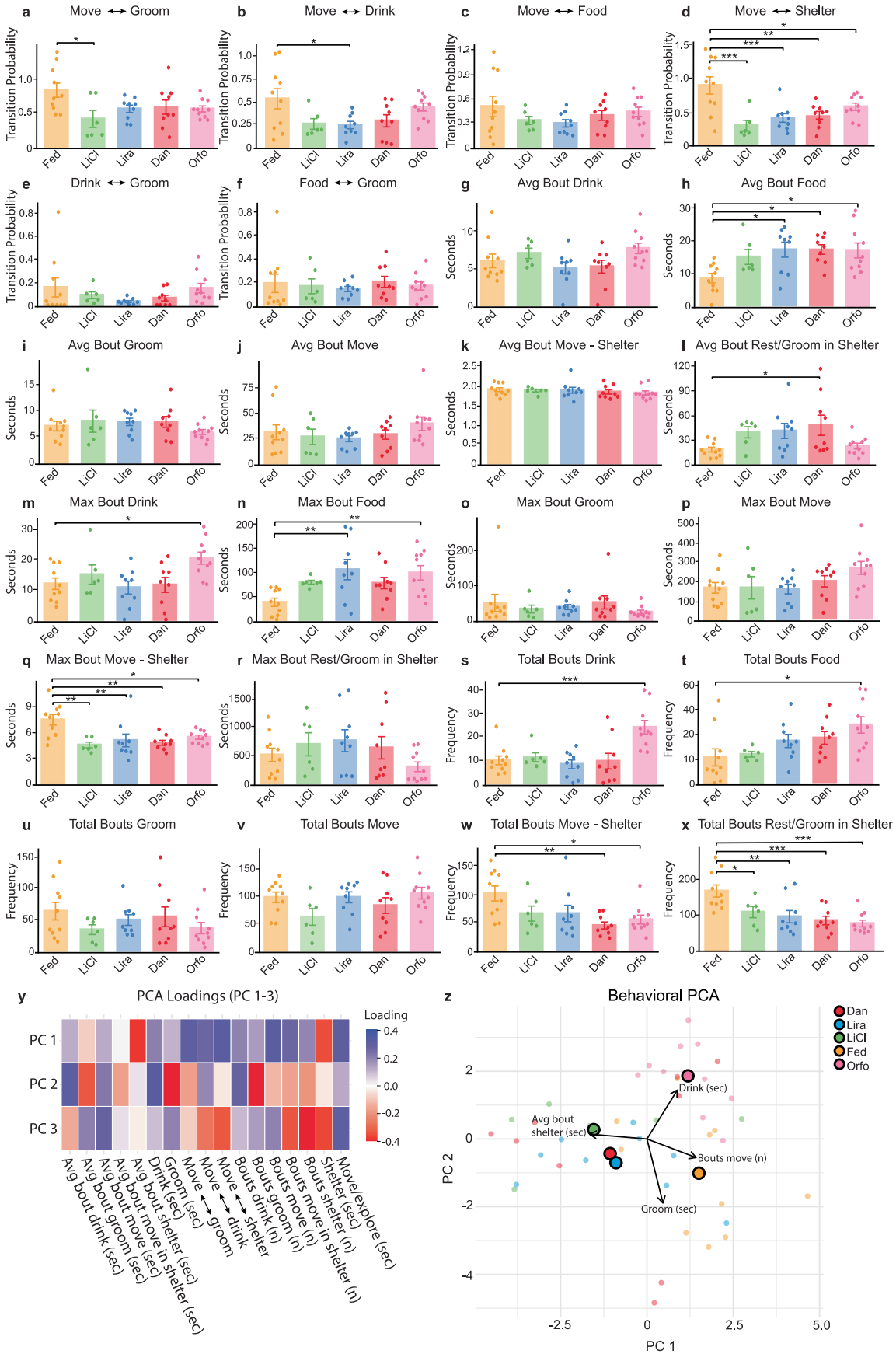

Extended Data Fig. 6 | See next page for caption.

Extended Data Fig. 6 | Behavioural transitions, bout characteristics and network PCA across treatment groups. a–f, Transition probabilities between behaviours for fed, LiCl-, liraglutide-, danuglipron-, or orforglipron-treated mice. Directionality of transitions was combined for simplicity. Statistical comparisons were performed using one-way ANOVA with Holm-corrected post-hoc pairwise tests comparing fed mice to each treatment group ($n = 10$ fed, $n = 6$ LiCl, $n = 9$ Lira, $n = 9$ Dan, $n = 10$ Orfo, $^{*}P < 0.05$; $^{**}P < 0.01$; $^{***}P < 0.001$). **g–l**, Average bout length (seconds) for each behaviour across conditions. **m–r**, Maximum bout length (seconds) observed per mouse during the recording period. **s–x**, Total number of behaviour bouts (frequency) across conditions. Statistical comparisons for panels g-x used one-way ANOVA with Holm correction as above. ($n = 10$ fed, $n = 6$ LiCl, $n = 9$ Lira, $n = 9$ Dan, $n = 10$ Orfo, $^{*}P < 0.05$; $^{**}P < 0.01$; $^{***}P < 0.001$). All data are mean ± s.e.m. **y**, PC loadings for behavioural features. Loadings for PC1, PC2, and PC3 are shown, with colour intensity indicating the strength and direction of behavioural contributions (blue = positive loading, red = negative loading). **z**, PCA of behavioural features excluding food-motivated behaviours. Arrows indicate the contribution of each behaviour to the PCs. For each PC, the top contributing behaviour in each direction is shown. Arrow direction reflects correlation with the PC, and length indicates the strength of contribution (scaled for visibility). All data are mean ± s.e.m.

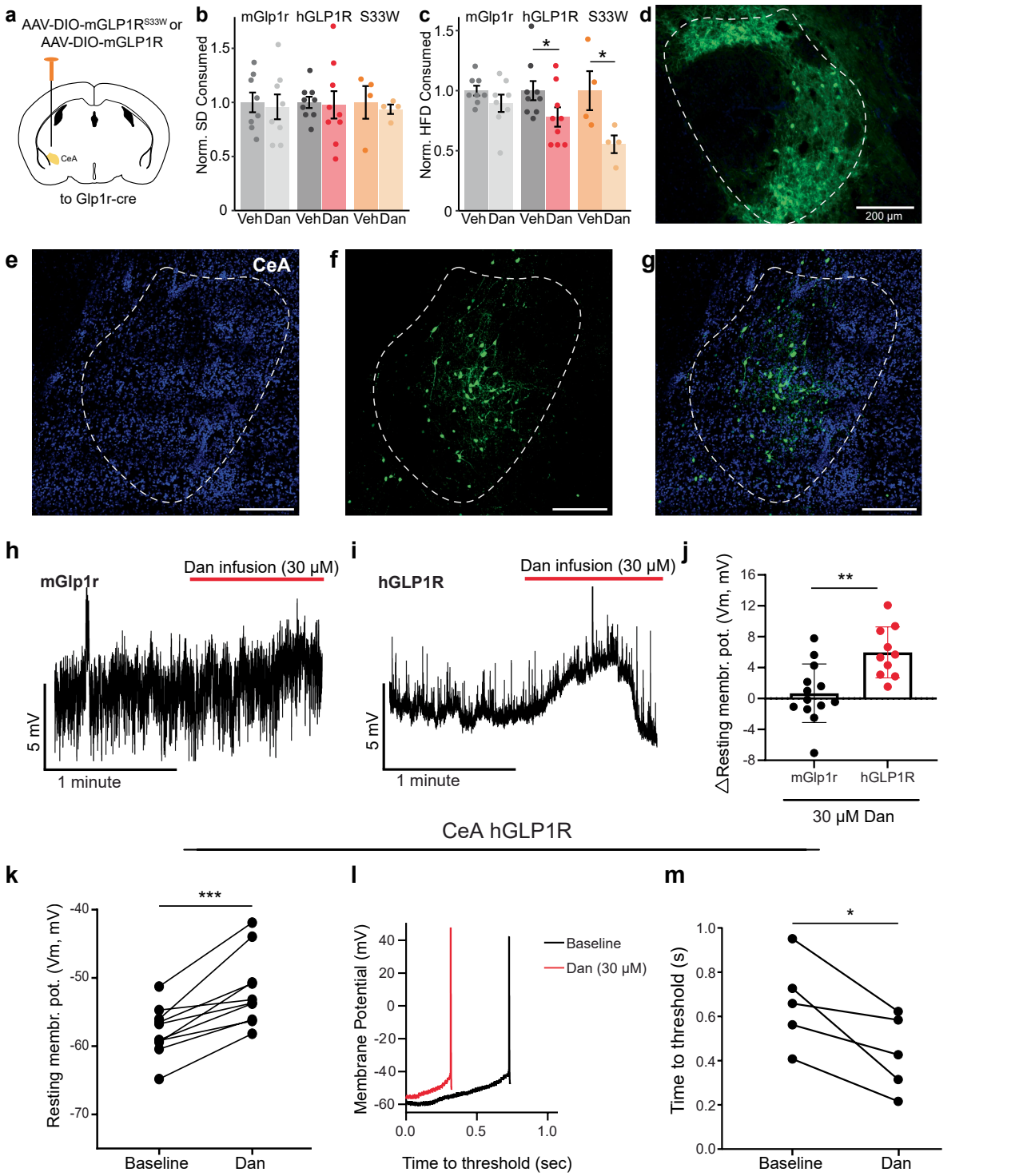

Extended Data Fig. 7 | Functional validation of AAV-DIO-hGLP1R and AAV-DIO-mGLP1R^{S33W}-HA and electrophysiological validation of AAV-DIO-hGLP1R in amygdala neurons. a, Schematic of Glp1r-Cre mice injected with a Cre-dependent AAV carrying full-length mouse Glp1r (mGlp1r) or AAV carrying full-length mouse GLP1R with the S33W mutation at position 33 (mGLP1R^{S33W}) in the CeA. **b**,**c**, Normalized 4-hour (**b**) SD and (**c**) HFD consumption post-injection of vehicle or danuglipron in mGlp1r, full-length human GLP1R (hGLP1R) or mGlp1r-S33W (S33W) expressing mice mGLP1R $n = 8$, hGLP1R $n = 9$, mGLP1R^{S33W} $n = 4$, two-way ANOVA with Bonferroni correction). **d**, Representative image of AAV-DIO-mGLP1R^{S33W}-HA expression in the CeA (green). Scale bars, 200 µm. **e**–**g**, Localization of eYFP-labelled hGLP1R-expressing neurons in the amygdala of Glp1r-Cre mice co-injected with AAV-DIO-hGLP1R and AAV-DIO-eYFP (scale bars, 100 µm). **h**,**i**, Representative traces showing the effect of danuglipron perfusion (Dan; 30 µM) on the resting membrane potential of **h**, control mGlp1r-expressing neurons from Glp1r-Cre mice injected with AAV-DIO-mGlp1r and AAV-DIO-eYFP, and **i**, hGLP1R-expressing neurons. **j**, Average depolarization induced by danuglipron in mGlp1r- or hGLP1R-expressing neurons (mGlp1r: 13 cells from 7 mice; hGLP1R: 10 cells from 7 mice, unpaired t-test). **k**, Resting membrane potential of hGLP1R-expressing neurons before (baseline) and after 30 µM danuglipron perfusion (10 cells, 7 mice, paired t-test). **l**, Representative action potential traces from a hGLP1R-expressing neuron evoked by a slow current injection ramp (100 pA/s) before and after danuglipron perfusion. **m**, Time to threshold quantification of hGLP1R-expressing neurons before and after danuglipron perfusion (5 cells, 4 mice, paired t-test). Data are mean ± s.e.m. $^{*}P < 0.05$; $^{**}P < 0.01$; $^{***}P < 0.001$.

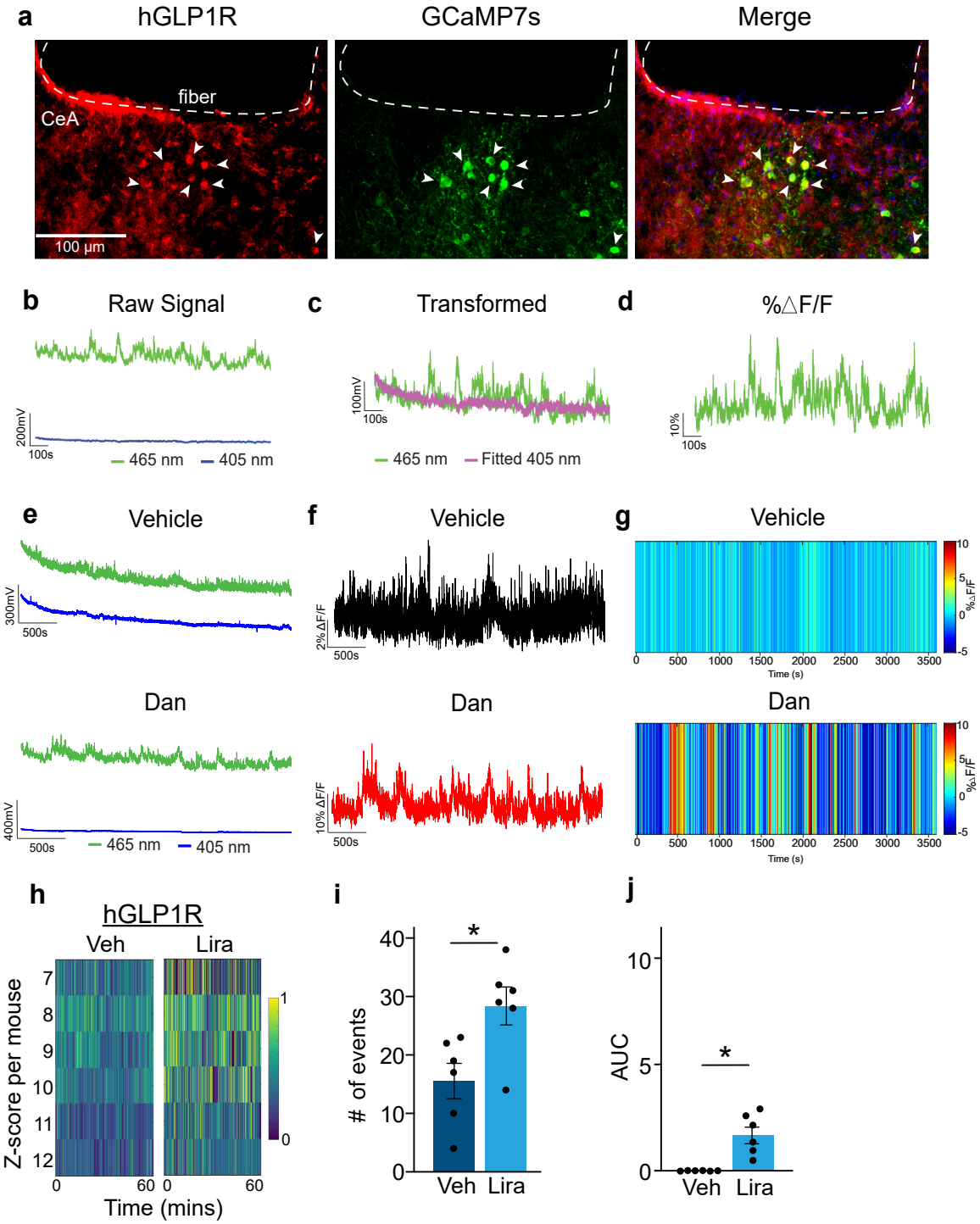

Extended Data Fig. 8 | Fibre photometry recordings and validation of CeA^{Glp1r} neurons. a, Representative images of AAV-DIO-GCaMP7s + hGLP1R targeted to the CeA. Validation with hGLP1R antibody (red; left), GCaMP7s (green; middle), and verification of colocalization (right). Scale bars, 100 µm. **b**, Representative traces of CeA^{Glp1r} fibre photometry recordings showing calcium-dependent fluorescence (465 nm) and calcium-independent, isosbestic fluorescence (405 nm) signals. **c**, Fitted 405 nm signal (pink) transformed for ΔF/F calculation. **d**, Representative trace of %ΔF/F used for *z*-score analysis. **e**, One-hour raw traces of CeA^{Glp1r} fibre photometry recordings under vehicle and danuglipron conditions. **f**, Analysed %ΔF/F traces corresponding to the recordings shown in **e**. **g**, Heat-map representation of %ΔF/F activity for both conditions. **h**, Heat maps of Z-scored neuronal calcium signals for each mouse during one hour of fibre photometry recording after vehicle (left) or liraglutide (right) injection in CeA-hGLP1R-expressing mice. **i**, Number of significant calcium events averaged per condition during 1-hour recording session following vehicle or liraglutide injection ($n = 6$ mice per injection, paired t-test). **j**, AUC quantification of calcium recordings ($n = 6$ mice per condition, paired t-test). Data are mean ± s.e.m. $^{*}P < 0.05$; $^{**}P < 0.01$; $^{***}P < 0.001$.

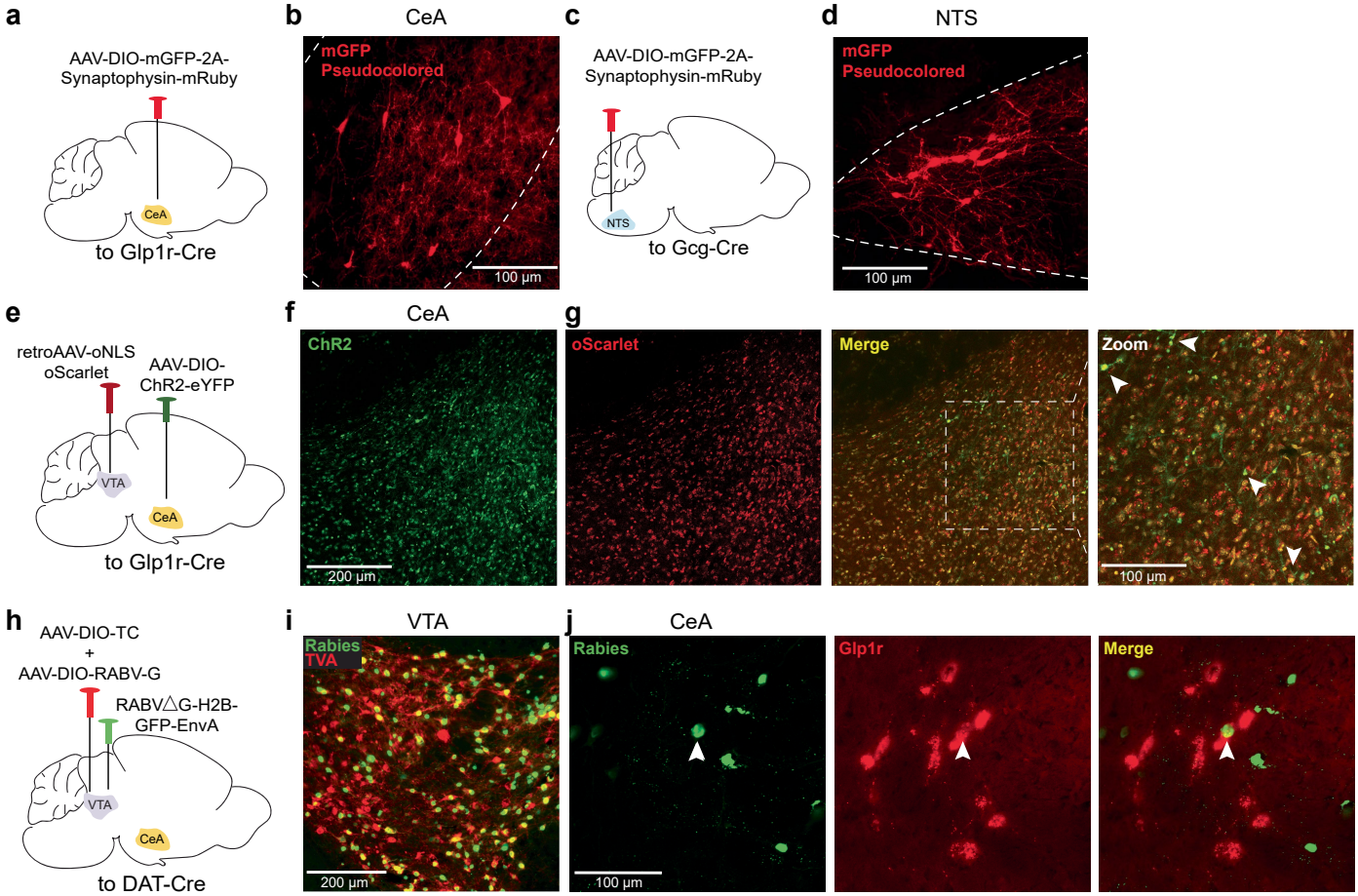

Extended Data Fig. 9 | Tracing from CeA to VTA reveals connections between CeA^{Glp1r} and VTA^{DAT} neurons. a,**c**, Illustrations of AAV-mediated synaptophysin tracing in Glp1r-Cre and Gcg-Cre mice injected with AAV-DIO-mGFP-2A-Synaptophysin-mRuby in the CeA (**a**) and NTS (**c**). **b**,**d**, Representative images showing mGFP (red, pseudocoloured mGFP) expression in the CeA^{Glp1r} (**b**) and NTS^{Gcg} (**d**) starter neurons (scale bars, 100 µm). **e**, Illustration of AAV-mediated retrograde tracing in Glp1r-Cre mice injected with retroAAV-oNLS-oScarlet in the VTA and Cre-dependent ChR2-eYFP in the CeA. **f**, Representative image showing ChR2-eYFP expression the CeA (scale bar, 200 µm). **g**, Representative images showing Left: oNLS-oScarlet expression in the CeA, Middle: merged image, Right: magnified view of the merged image; arrowheads mark Glp1r neurons colocalized with oNLS-oScarlet expression (scale bar, 100 µm). **h**, Illustration of cell-type specific, monosynaptic retrograde rabies tracing approach targeting VTA dopamine neurons. **i**, Representative image showing the VTA injection site in Dat-Cre mice (scale bar, 200 µm). **j**, Left: GFP+ input neurons identified in the CeA. Middle: In situ hybridization for Glp1r mRNA in the CeA. Right: merged image demonstrating colocalization (white arrow) of Glp1r mRNA with rabies-derived GFP in the CeA (10.9% ± 1.7% Glp1r neurons in the CeA are positive for rabies expression, n = 4 mice; scale bar, 100 µm).

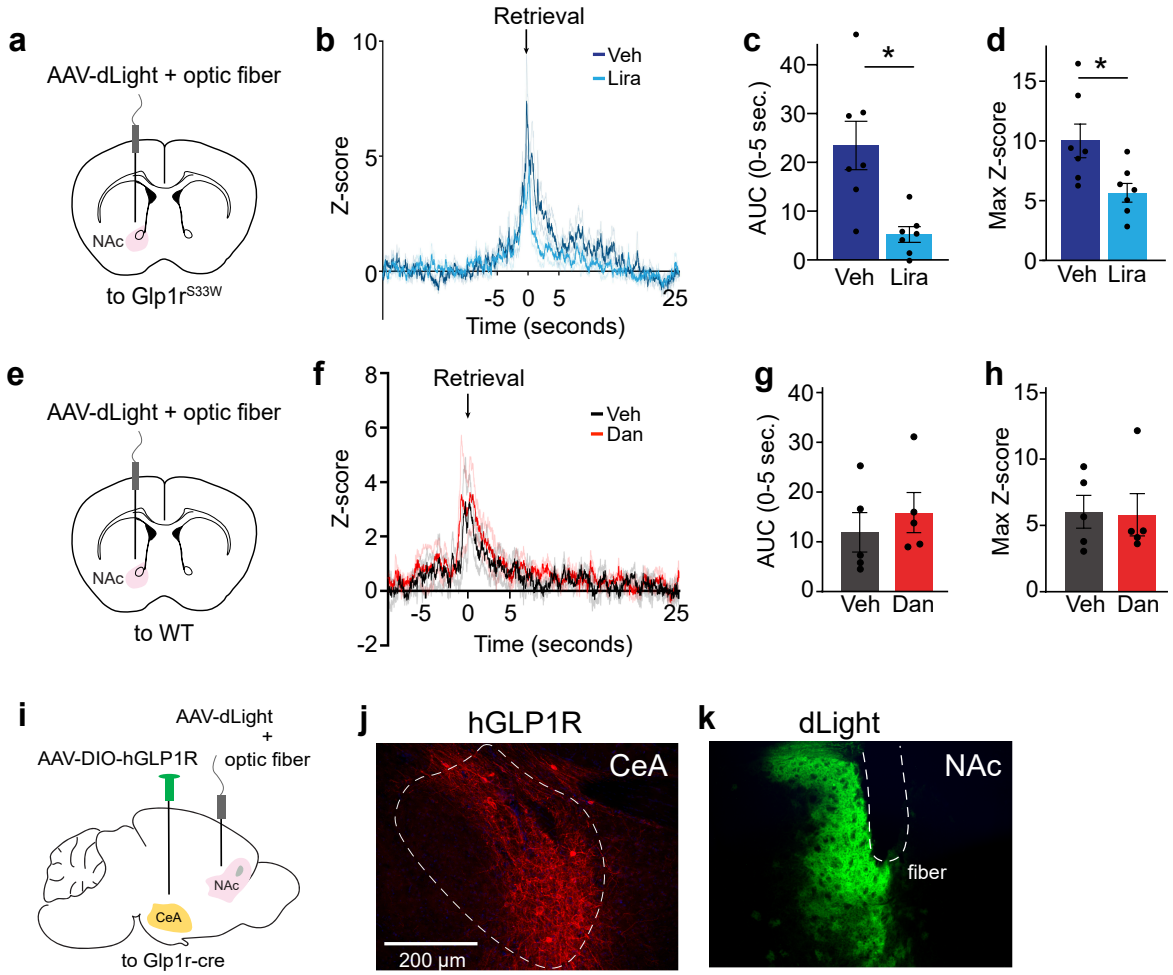

Extended Data Fig. 10 | Liraglutide reduces NAc dopamine release in response to HFD, and WT mice do not respond to danuglipron. a, Schematic of genetically encoded dopamine sensor, AAV-dLight1.3b, injection and fibre-optic implant in the NAc of *Glp1r*^{S33W} mice. **b**, Averaged Z-score traces showing dopamine release in the NAc in response to HFD following administration of vehicle or liraglutide in *Glp1r*^{S33W} mice. Traces are aligned to food retrieval time (t = 0) and averaged across five food trials per mouse. **c**,**d**, Quantified (**c**) AUC for Z-scores and (**d**) maximum fluorescence Z-scores within the food retrieval window ($n = 7$, paired t-test). **e**, Schematic of AAV-dLight1.3b injection and fibre-optic implant in the NAc of WT mice. **f**, Averaged Z-score traces showing dopamine release in the NAc in response to HFD following administration of vehicle or danuglipron in WT mice. Traces are aligned to food retrieval time (t = 0) and averaged across five food trials per mouse. **g**,**h**, Quantified (**g**) AUC for Z-scores and (**h**) maximum fluorescence Z-scores within the food retrieval window ($n = 5$ per injection, paired t-test). **i**, Schematic showing AAV-dLight1.3b injection into the NAc and AAV-DIO-hGLP1R injection into the CeA of Glp1r-Cre mice, with fibre-optic implants in the NAc. **j**, Validation of AAV-DIO-hGLP1R targeting the CeA using hGLP1R antibody staining (red). **k**, Representative AAV-dLight expression in the NAc and fibre-optic implant placement (green). Scale bars, 200 µm. Data are mean ± s.e.m. $^{*}P < 0.05$; $^{**}P < 0.01$; $^{***}P < 0.001$.

nature portfolio

Corresponding author(s): Chris Deppmann and Ali D. Guler

Last updated by author(s): Feb 24, 2025

Reporting Summary

Nature Portfolio wishes to improve the reproducibility of the work that we publish. This form provides structure for consistency and transparency in reporting. For further information on Nature Portfolio policies, see our Editorial Policies and the Editorial Policy Checklist.

Statistics

For all statistical analyses, confirm that the following items are present in the figure legend, table legend, main text, or Methods section.

n/a	Confirmed	
☐	☒	The exact sample size (*n*) for each experimental group/condition, given as a discrete number and unit of measurement
☐	☒	A statement on whether measurements were taken from distinct samples or whether the same sample was measured repeatedly
☐	☒	The statistical test(s) used AND whether they are one- or two-sided *Only common tests should be described solely by name; describe more complex techniques in the Methods section.*
☒	☐	A description of all covariates tested
☐	☒	A description of any assumptions or corrections, such as tests of normality and adjustment for multiple comparisons
☐	☒	A full description of the statistical parameters including central tendency (e.g. means) or other basic estimates (e.g. regression coefficient) AND variation (e.g. standard deviation) or associated estimates of uncertainty (e.g. confidence intervals)
☐	☒	For null hypothesis testing, the test statistic (e.g. *F*, *t*, *r*) with confidence intervals, effect sizes, degrees of freedom and *P* value noted *Give P values as exact values whenever suitable.*
☒	☐	For Bayesian analysis, information on the choice of priors and Markov chain Monte Carlo settings
☒	☐	For hierarchical and complex designs, identification of the appropriate level for tests and full reporting of outcomes
☒	☐	Estimates of effect sizes (e.g. Cohen's *d*, Pearson's *r*), indicating how they were calculated

Our web collection on statistics for biologists contains articles on many of the points above.

Software and code

Policy information about availability of computer code

Data collection	CLAX (columbus instruments) for metabolic parameters monitoring; Doric Neuroscience Studio (Doric lenses) for fiber photometry recording; EthoVision XT and MediaRecorder for Phenotyper recordings (Noldus) ClampFit 11.2
Data analysis	Microsoft Excel (2024), GraphPad Prism (v10.4.0), Adobe Illustrator CC (v28.3) for preparation of figures; Python (v3.11.5) within the JupyterLab environment (v3.6.3), MATLAB R2023a and RStudio (v4.3.0) for data analysis; Doric Neuroscience Studio (v6.5.0.0) for fiber photometry data analysis; Image J (v1.54m), CellProfiler for image processing; Oxymax (columbus instruments) for metabolic parameters data analysis; Additional code is available at https://github.com/UVACircMetNeuLab/glp1r-reward-circuit

For manuscripts utilizing custom algorithms or software that are central to the research but not yet described in published literature, software must be made available to editors and reviewers. We strongly encourage code deposition in a community repository (e.g. GitHub). See the Nature Portfolio guidelines for submitting code & software for further information.

Data

Policy information about availability of data

All manuscripts must include a data availability statement. This statement should provide the following information, where applicable:

- Accession codes, unique identifiers, or web links for publicly available datasets
- A description of any restrictions on data availability
- For clinical datasets or third party data, please ensure that the statement adheres to our policy

Data and code available on LabArchives at https://mynotebook.labarchives.com/share/Guler%2520Lab%2520Notebook/MTQuM3wxMTY0NDYxLzExL1RyZWVOb2RlLzI1NDM4MDU2N3wzNi4z or on Github at https://github.com/UVACircMetNeuLab/glp1r-reward-circuit.

Research involving human participants, their data, or biological material

Policy information about studies with human participants or human data. See also policy information about sex, gender (identity/presentation), and sexual orientation and race, ethnicity and racism.

Reporting on sex and gender	No humans participants in this study
Reporting on race, ethnicity, or other socially relevant groupings	No humans participants in this study
Population characteristics	No humans participants in this study
Recruitment	No humans participants in this study
Ethics oversight	No humans participants in this study

Note that full information on the approval of the study protocol must also be provided in the manuscript.

Field-specific reporting

Please select the one below that is the best fit for your research. If you are not sure, read the appropriate sections before making your selection.

☒ Life sciences ☐ Behavioural & social sciences ☐ Ecological, evolutionary & environmental sciences

For a reference copy of the document with all sections, see nature.com/documents/nr-reporting-summary-flat.pdf

Life sciences study design

All studies must disclose on these points even when the disclosure is negative.

Sample size	Sample sizes were based on prior experience with similar experiments. For behavioral and metabolic studies, we aimed for a minimum of 10 animals per group when possible. While we did not perform a formal power analysis for each experiment in this study, previous analyses in our lab (using Cohen's d) have shown that, with $\alpha = 0.05$ and power = 0.8, a sample size of ~6 animals per group is sufficient to detect a ~40% difference in mean with ~25% standard deviation, and ~12 animals are sufficient to detect a ~20% difference in mean with ~20% standard deviation. Sample sizes in this study therefore ranged from 6 to 12 animals per group.
Data exclusions	Animals were excluded if histological validation revealed mistargeted viral injections and/or fiber optic implant or lack of expression of the intended payload in the targeted brain region. This was determined post hoc through brain section analysis. For electrophysiology experiments, cells with unstable resting membrane potentials were excluded from the analysis and no cells were considered statistical outliers. For behavior in Phenotyper chambers, mice that failed to meet a baseline criterion of ≥50 food hopper head entries between ZT 12–14 were excluded to ensure sufficient engagement with the feeding setup. Of 59 mice tested, 12 did not meet this threshold and were excluded.
Replication	All experiments were independently replicated at least twice, and reproducibility was confirmed. Data from biological replicates were combined for final analysis and presentation.
Randomization	Animals were randomly assigned to experimental or control groups. For behavioral experiments, littermates were randomly distributed across conditions. When feasible, both control and treatment groups were tested simultaneously. The positions of animals in behavioral testing chambers were also randomized to prevent spatial bias.
Blinding	Blinding was not performed due to the limited number of researchers with the required expertise to carry out the experiments and interpret the data. However, we took care to ensure consistent experimental outcomes across replicates and relied on objective quantification methods (e.g., electrophysiology traces, automated behavioral readouts) to reduce subjectivity in data analysis.

Reporting for specific materials, systems and methods

We require information from authors about some types of materials, experimental systems and methods used in many studies. Here, indicate whether each material, system or method listed is relevant to your study. If you are not sure if a list item applies to your research, read the appropriate section before selecting a response.

Materials & experimental systems

n/a	Involved in the study
☐	☒ Antibodies
☒	☐ Eukaryotic cell lines
☒	☐ Palaeontology and archaeology
☐	☒ Animals and other organisms
☒	☐ Clinical data
☒	☐ Dual use research of concern
☒	☐ Plants

Methods

n/a	Involved in the study
☒	☐ ChIP-seq
☒	☐ Flow cytometry
☒	☐ MRI-based neuroimaging

Antibodies

Antibodies used

All relevant information regarding the antibodies used is provided in the Methods section. The following primary antibodies were used for fluorescent labeling: anti-c-Fos (rabbit, 1:1000; Synaptic Systems, #226003, RRID:AB_2231974), anti-DsRed (rabbit, 1:1000; Takara Bio, catalog no. 632496, RRID:AB_10013483), anti-TdTomato (goat, 1:1000; Arigobio, catalog no. ARG55724), anti-hGLP1R (rabbit, 1:200; Invitrogen, catalog no. PA5-97789, RRID: AB_2812404), anti-HA (rabbit, 1:1000, Cell Signaling, catalog no. 3724), anti-Th (rabbit, 1:500; Chemicon, catalog no. AB152), and anti-GFP (goat, 1:500; Rockland, catalog no. 600-101-215). The secondary antibodies (Jackson ImmunoResearch) used were Cy2-conjugated donkey anti-rabbit (1:250; catalog no. 711-225-152, RRID:AB_2340612), Cy3-conjugated donkey anti-rabbit (1:250; catalog no. 711-165-152, RRID:AB_2307443), Cy5-conjugated donkey anti-rabbit (1:250; catalog no. 711-175-152, RRID:AB_2340607), Cy3-conjugated donkey anti-goat (1:250; catalog no. 705-165-147, RRID:AB_2307351), and Alexa-Fluor® 488 donkey anti-goat (1:250; catalog no. 705-545-003, RRID:AB_2340428).

Validation

All primary antibodies used contain RRID and have been validated for immunohistochemistry by the specific vendor and confirmed in our lab. Also, most of them have been validated in our previous publications. For anti-hGLP1R (Invitrogen, catalog no. PA5-97789, RRID: AB_2812404) we validate the antibody by comparing to tissue that does not express hGLP1R.
1) Anti-DsRed (rabbit, 1:1000; Takara Bio, catalog no. 632496, RRID:AB_10013483)
https://www.takarabio.com/products/antibodies-and-elisa/fluorescent-protein-antibodies/red-fluorescent-protein-antibodies?srsltid=AfmBOoqD91H3-b532bZmFEbmZhP2af8p6iNTVibmkLsKFiGD-gF8fPyY
2) anti-TdTomato (goat, 1:1000; Arigobio, catalog no. ARG55724)
https://www.arigobio.com/anti-tdTomato-antibody-ARG55724.html
3) anti-hGLP1R (rabbit, 1:200; Invitrogen, catalog no. PA5-97789, RRID: AB_2812404)
https://www.thermofisher.com/antibody/product/GLP1R-Antibody-Polyclonal/PA5-97789
4) anti-HA (rabbit, 1:1000, Cell Signaling, catalog no. 3724)
https://www.cellsignal.com/products/primary-antibodies/ha-tag-c29f4-rabbit-monoclonal-antibody/3724?srsltid=AfmBOop53B9GSxUDmSteNbLtMokdrpydLCLIf9CswdIAp86HB7bTsoRe
5) anti-Th (rabbit, 1:500; Chemicon, catalog no. AB152)
https://www.sigmaaldrich.com/US/en/product/mm/ab152?srsltid=AfmBOop81-1Y0UfCXvLd2x5JIrryQe4syIGPogRy_T4r62ZyFngwtjgv
6) anti-GFP (goat, 1:500; Rockland, catalog no. 600-101-215)
https://www.thermofisher.com/antibody/product/GFP-Antibody-Polyclonal/600-101-215M
Note: anti-c-Fos (rabbit, 1:1000; Synaptic Systems, #226003, RRID:AB_2231974) has been discontinued but well validated before. Example: Zan et al., 2025, Neuron, PMID: 41043420

Animals and other research organisms

Policy information about studies involving animals; ARRIVE guidelines recommended for reporting animal research, and Sex and Gender in Research

Laboratory animals

We used 8-week or older male and female mice. Strains information:
1) C57BL/6J (Strain #:000664, RRID:IMSR_JAX:000664)
2) Glp1r-ires-Cre (STOCK Glp1rtm1.1(cre)Lbrl/RcngJ, Strain #:029283, RRID:IMSR_JAX:029283)
3) Glp1r S33W mice have been generated in this study and available on JAX (STOCK Glp1rem1Aglu/J, Strain #:040551 RRID:IMSR_JAX:040551
4) Dat-ires-Cre (B6.SJL-Slc6a3tm1.1(cre)Bkmn/J, Strain #:006660, RRID:IMSR_JAX:006660)
5) Gcg-Cre mice (C57BL/6J-Tg(Gcg-cre)-1Mmsc/Mmmh, stock #051056-MU, RRID:MMRRC_051056-MU)
6) Ai14 tdTomato reporter line (B6.Cg-Gt(ROSA)26Sortm14(CAG-tdTomato)Hze/J, strain #007914, RRID:IMSR_JAX:007914)
7) Glp1r flox/flox mice (B6(SJL)-Glp1rtm1.1Stof/J, strain #035238, RRID:IMSR_JAX:035238)

Wild animals

No wild animals were used in this study.

Reporting on sex	We used both male and female mice for most experiments. In cases where a specific sex was excluded, a scientific rationale is provided. Full details are available in the main text and Methods section.
Field-collected samples	No field-collected samples were used in this study.
Ethics oversight	All experiments were conducted in compliance with the Association for Assessment of Laboratory Animal Care policies and approved by the Institutional Animal Care and Use Committees of the University of Virginia, University of Washington, and University of California, Irvine.

Note that full information on the approval of the study protocol must also be provided in the manuscript.

Plants

Seed stocks	No plants were used in this study
Novel plant genotypes	No plants were used in this study
Authentication	No plants were used in this study